Extraordinary Biomass-Burning Episode and Impact Winter Triggered by the Younger Dryas Cosmic Impact ~12,800 Years Ago. 1. Ice Cores and Glaciers

Article *in* The Journal of Geology · February 2018

DOI: 10.1086/695703

CITATIONS
55

READS
6,389

27 authors, including:

Joanne P Ballard
Czech Academy of the Sciences
23 PUBLICATIONS **166** CITATIONS

SEE PROFILE

A.V Adedeji
Elizabeth City State University
56 PUBLICATIONS **651** CITATIONS

SEE PROFILE

Ted E. Bunch
Retired
267 PUBLICATIONS **6,453** CITATIONS

SEE PROFILE

Extraordinary Biomass-Burning Episode and Impact Winter Triggered by the Younger Dryas Cosmic Impact ~12,800 Years Ago. 1. Ice Cores and Glaciers

Wendy S. Wolbach,[1,*] *Joanne P. Ballard,*[2] *Paul A. Mayewski,*[3] *Victor Adedeji,*[4] *Ted E. Bunch,*[5] *Richard B. Firestone,*[6] *Timothy A. French,*[1] *George A. Howard,*[7] *Isabel Israde-Alcántara,*[8] *John R. Johnson,*[9] *David Kimbel,*[10] *Charles R. Kinzie,*[1] *Andrei Kurbatov,*[3] *Gunther Kletetschka,*[11] *Malcolm A. LeCompte,*[12] *William C. Mahaney,*[13] *Adrian L. Melott,*[14] *Abigail Maiorana-Boutilier,*[15] *Siddhartha Mitra,*[15] *Christopher R. Moore,*[16] *William M. Napier,*[17] *Jennifer Parlier,*[18] *Kenneth B. Tankersley,*[19] *Brian C. Thomas,*[20] *James H. Wittke,*[5] *Allen West,*[18,†] *and James P. Kennett*[21]

ABSTRACT

The Younger Dryas boundary (YDB) cosmic-impact hypothesis is based on considerable evidence that Earth collided with fragments of a disintegrating ≥100-km-diameter comet, the remnants of which persist within the inner solar system ~12,800 y later. Evidence suggests that the YDB cosmic impact triggered an "impact winter" and the subsequent Younger Dryas (YD) climate episode, biomass burning, late Pleistocene megafaunal extinctions, and human cultural shifts and population declines. The cosmic impact deposited anomalously high concentrations of platinum over much of the Northern Hemisphere, as recorded at 26 YDB sites at the YD onset, including the Greenland Ice Sheet Project 2 ice core, in which platinum deposition spans ~21 y (~12,836–12,815 cal BP). The YD onset also exhibits increased dust concentrations, synchronous with the onset of a remarkably high peak in ammonium, a biomass-burning aerosol. In four ice-core sequences from Greenland, Antarctica, and Russia, similar anomalous peaks in other combustion aerosols occur, including nitrate, oxalate, acetate, and formate, reflecting one of the largest biomass-burning episodes in more than 120,000 y. In support of widespread wildfires, the perturbations in CO_2 records from Taylor Glacier, Antarctica, suggest that biomass burning at the YD onset may have consumed ~10 million km^2, or ~9% of Earth's terrestrial biomass. The ice record is consistent with YDB impact theory that extensive impact-related biomass burning triggered the abrupt onset of an impact winter, which led, through climatic feedbacks, to the anomalous YD climate episode.

Online enhancements: appendix.

Introduction

Firestone et al. (2007) initially posited that exotic materials found in the Younger Dryas boundary (YDB) layer provide evidence of a major cosmic-impact event, caused by Earth's collision with a cometary swarm ~12,800 calendar years ago at the onset of the Younger Dryas (YD) climate episode. Studies of >40 sedimentary sequences distributed across North and South America, western Europe, and western Asia document peaks in exotic YDB materials, including high-temperature iron-rich spherules; silica-rich glassy spherules; meltglass; and nanodiamonds, iridium, platinum (fig. A1; figs. A1 and A2 are available online), and osmium (tables A1, A2; tables A1–A4 are available online). Independent groups have confirmed much of the YDB impact evidence, but others have not or have offered alternate explanations. It is not the intent of this contribution to review and discuss previous publications concerning the YDB impact proxies, and so a comprehensive bibliography is provided in table A3.

Many YDB sites exhibit evidence of a distinct peak in biomass burning associated with the YDB impact-related proxies. Part 1 of this contribution

Manuscript received September 11, 2017; accepted September 14, 2017; electronically published February 1, 2018.

* The authors' affiliations can be found at the end of the article.

† Author for correspondence; e-mail: allen7633@aol.com.

[The Journal of Geology, 2018, volume 126, p. 000–000] 0022-1376/2018/12602-0002$15.00. DOI: 10.1086/695703

(this article) summarizes evidence of biomass burning in global ice-sheet records, and part 2 (Wolbach et al. 2018) summarizes sedimentary records that contain biomass-burning evidence, including aciniform carbon (AC/soot), black carbon/soot, charcoal, carbon spherules, and glass-like carbon. For a site map, see figure 1; for descriptions and images of YDB biomass-burning proxies, see Wolbach et al. (2018), especially figures A1–A6 and "Biomass-Burning Proxies Found at YDB Sites" in the appendix).

Peaks in impact-related biomass-burning proxies, such as AC/soot, have been identified in at least four previously documented cosmic-impact events: Sudbury, Mjølnir, Manson, and Cretaceous-Tertiary (K-Pg; "Biomass Burning in Previous Cosmic-Impact Events" in the appendix, available online). Furthermore, it is widely accepted that biomass burning during the K-Pg impact event initiated a severe climate change known as "impact winter" ("Biomass Burning in Previous Cosmic-Impact Events"). The K-Pg impact layer broadly contains peaks in diverse biomass-burning proxies, including AC/soot (Wolbach and Anders 1989), charcoal (Belcher et al. 2003; Robertson et al. 2004), and carbon spherules (Adatte et al. 2005). As evidence of a high-temperature event, these biomass-burning proxies are also associated with peaks in high-temperature impact-related proxies, including magnetic spherules (Adatte et al. 2005), meltglass (Adatte et al. 2005), and nanodiamonds (Carlisle and Braman 1991). Kaiho et al. (2016) proposed that the K-Pg impact produced enough AC/soot and dust to block sunlight and trigger a major climate change (impact winter) that, in turn, degraded entire ecosystems and contributed to the severe K-Pg mass extinctions.

The much more recent Tunguska impact event in 1908 involved a meteorite/comet that detonated ~15 km in the atmosphere over Siberia, toppled 80 million trees, and triggered biomass burning (Florenskiy 1965). The discovery of high-temperature meltglass near the epicenter of the airburst indicates sufficiently high temperature to initiate biomass burning (a minimum of 1200°C; Kirova and Zaslavskaya 1966; Bunch et al. 2012).

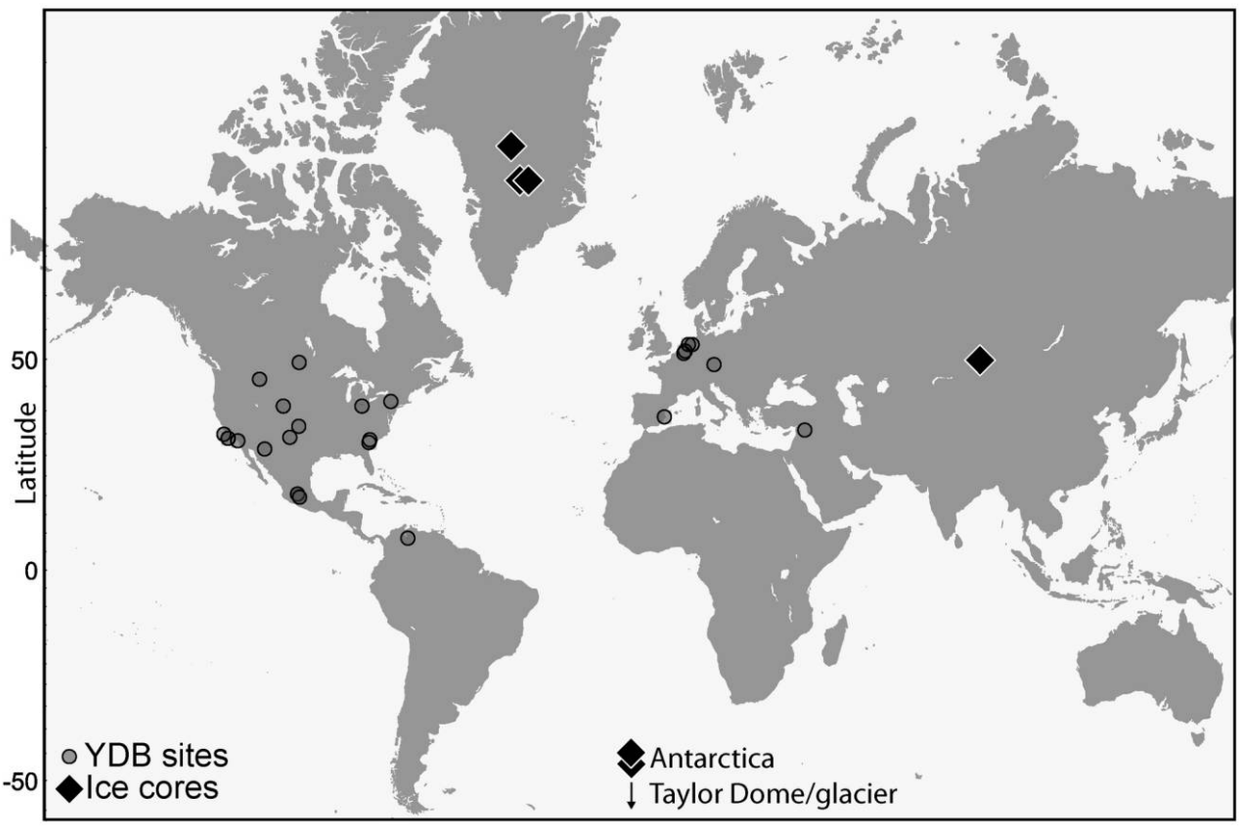

Figure 1. Locations for ice cores and Younger Dryas boundary (YDB) sites with peak biomass-burning proxies. Black diamonds represent 6 ice records that display chemical proxies in support of anomalously high YDB biomass burning. Taylor Dome and Taylor Glacier are off the map in Antarctica. Circles represent 23 sites with a documented YDB layer containing peaks in biomass-burning proxies.

The onset of YD cooling at ~12,800 cal BP represented an abrupt climatic event that was most strongly expressed in the North Atlantic region, where temperatures plunged ~8°C (Carlson 2013). The commonly accepted explanation for YD cooling is that iceberg calving and meltwater flooding capped the North Atlantic, thereby shutting down thermohaline circulation (Broecker 1997). Diminution of sunlight by dust loading and shifts in atmospheric circulation have been proposed as additional causes of YD climate change by Renssen et al. (2015), whose numerical simulations indicate that all three mechanisms were required to trigger YD cooling. The YDB impact theory adds an additional key element by suggesting that these climate-changing mechanisms did not occur randomly but rather were triggered by the YDB impact event. After shutdown of the ocean conveyor, the YD episode persisted for another ~1400 years, not because of continued airburst/impacts but because, once circulation stopped, feedback loops and inertia within the ocean system maintained the changed state of circulation until it reverted to its previous state (Firestone et al. 2007; Kennett et al. 2018).

Independently published studies of biomass-burning aerosols in three Greenland ice cores have previously shown that a large episode of biomass burning closely coincided with the onset of YD cooling (Legrand et al. 1992; Mayewski et al. 1993, 1997; Fischer et al. 2015). Recognition of the magnitude and timing of this event in the Greenland ice sheet was a major factor in Firestone et al.'s (2007) inference that an episode of biomass burning was triggered by an impact event at the YD onset. Later, support for the original hypothesis came from the discovery of peaks in impact-related proxies in YDB ice samples collected at the margin of the Greenland ice sheet (Kurbatov et al. 2010).

Because of excellent preservation and minimal contamination, the Greenland ice sheet is an ideal repository of aerosols, representing a detailed record of wildfire activity in the Northern Hemisphere over the past hundred thousand years (Mayewski et al. 1993). Examples of combustion aerosols detected in ice cores and correlated with biomass-burning activity include ammonium (NH_4), nitrate (NO_3), levoglucosan (Kehrwald et al. 2012), acetate, oxalate, and formate (Legrand et al. 1992, 2016; Mayewski et al. 1993, 1996, 1997; Whitlow et al. 1994; Taylor et al. 1996; Fuhrer and Legrand 1997). Eichler et al. (2011) correlated ice-core aerosols with known historical wildfire episodes, including the one caused by the Tunguska impact event, and found that NH_4, NO_3, and potassium (K) are especially robust proxies of biomass-burning episodes. Similarly, Fuhrer and Legrand (1997) found that wildfires account for up to 40% of Holocene NH_4 concentrations in Greenland ice records, with the remainder derived mostly from marine and continental sources, including plant and microbial biomass.

Melott et al. (2010) proposed that some ice-core NH_4 at the YD onset was produced by the high-temperature and high-pressure passage of cometary fragments through Earth's atmosphere. Similarly, they suggested that airborne impact ejecta could have produced nitrates (NO_x) that were deposited in polar ice cores (Parkos et al. 2015; Melott et al. 2016). These two bolide-related hypotheses for the formation of combustion aerosols are not mutually exclusive with aerosol production by impact-related wildfires.

In this contribution, we summarize evidence in multihemispheric ice sequences in support of a widespread peak in biomass-burning activity at or close to the onset of the YD climate episode. We then examine the potential temporal relationship among the peaks in biomass burning, YD climate change, and the YDB extraterrestrial-impact event, as recorded in these ice sequences. The investigations of temporal relationships among these events can determine whether the hypothesis of causality (i.e., an impact trigger) is plausible or can be rejected.

Methods

The original ice-core data analyzed in this study were compiled from a number of independent sources (see "Sources of Ice-Core Data" in the appendix; table A4); no new ice-core data are presented in this contribution. The original data used multiple, incompatible age scales that prevent intercore comparisons and hence require recalibration ("Age-Depth Issues with Greenland Ice Cores" in the appendix). In addition, ice-core ages reported in years before AD 2000 (b2k) are incompatible with calibrated radiocarbon ages reported in years before AD 1950 (cal BP), a difference of 50 y. To address these issues, we converted all ice ages to the common Greenland Ice Core Chronology 2005 (GICC05) timescale (b2k; Rasmussen et al. 2008; Seierstad et al. 2014), with uncertainties of $\pm$140 y. We then subtracted 50 y to convert the ages to cal BP (relative to AD 1950), to permit comparison of the timescales of previously existing ice records here in part 1 with those of sedimentary terrestrial records in part 2 (Wolbach et al. 2018).

The compiled data are plotted with standard analytical methods and are typically presented in both raw and smoothed formats. For the latter, data points

were lowess-smoothed with half-windows of ~50–1000 y, depending on data density in each ice core, with fewer data points requiring larger smoothing windows.

Results

Correlation of Greenland Ice Sheet Project 2 Platinum with Onset of the YD Climate Episode. An anomalously high peak in Pt concentrations recorded in sediments and ice has been reported at or close to the YD onset across North America, western Europe, and western Asia at 26 sites (fig. A1), including an additional eight in this contribution. Petaev et al. (2013) initially discovered this Pt peak spanning ~21 y that began precisely at the onset of the YD climate episode in the Greenland Ice Sheet Project 2 (GISP2) ice core (see fig. 1). They attributed this episode of continuous Pt deposition to "multiple injections of Pt-rich dust into the stratosphere" by an estimated 800-m-diameter iron asteroid (Petaev et al. 2013, p. 1). This ice-core Pt-rich interval is especially significant because the chronology is well resolved to ~3 y per ice sample, as a result of higher accumulation rates and subannual layering. This resolution is much higher than nearly all terrestrial YDB stratigraphic sequences. Pt-rich sediment and Pt-rich spherules have also been reported in YDB-age sediment (Andronikov et al. 2014, 2015, 2016*a*, 2016*b*; Andronikov and Andronikova 2016; Moore et al. 2017; see "Widespread YDB Platinum Deposition" in the appendix).

Quantifying Sea Salt and Continental Dust. To test the hypothesis that peak Pt concentrations are synchronous with the onset of YD climate change, we analyzed GISP2 abundances of sea salt and continental dust (Cl, Ca, Na, Mg, and K) that mark the YD onset. Two of the key indicators of oceanic sea-salt transport in Greenland ice are chlorine (Cl) and sodium (Na), with ~99% of the latter being of marine origin (de Angelis et al. 1997). Concentrations of these elements increased sharply at the YD onset in response to an abrupt, major rise in wind strength caused by the shift in atmospheric circulation (Fuhrer and Legrand 1997; Mayewski et al. 1997). Dust from continental sources is dominated by magnesium, sulfate, and calcium (Ca), the latter of which is nearly 100% continental in origin (Fuhrer and Legrand 1997; Mayewski et al. 1997). Elevated abundances of these elements in Greenland ice reflect the enhanced transport of continental dust to the ice sheet, resulting from increases in wind strength and/or terrestrial aridity. Because dust transport typically increases at the onset of colder intervals (Ram and Koenig 1997), the abundances of these elements have been used to identify the YD climate shift within the Greenland ice cores (Fuhrer and Legrand 1997; Mayewski et al. 1997).

The results reveal that cumulative GISP2 concentrations of Cl, Ca, Na, Mg, and K rose abruptly by a factor of ~4 to a major peak at ~12,836 cal BP (fig. 2), marking the onset of a general trend in increasing windiness beginning at the YD onset. This increase began in the depth interval from 1712.70 to 1712.60 m, corresponding to the sudden increase of Pt concentrations (1712.625–1712.5 m). Hence, the record shows that the cumulative dust peak is essentially synchronous with the initial rise in Pt deposition (Petaev et al. 2013). Furthermore, this dust peak at the onset of the YD is outstanding in the entire ice-core record, being higher than 99.7% of values in the previous 100,000 y (not plotted).

Correlation of YD Climate Change and Biomass Burning. To test the hypothesis that the YDB impact event initiated widespread biomass burning and simultaneously triggered YD climate change, we compiled and analyzed >106,000 independently acquired data points for combustion-related aerosols (e.g., NH_4,

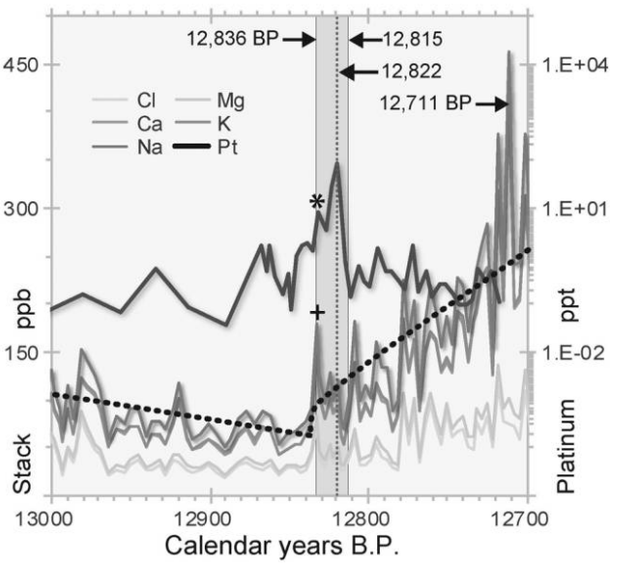

Figure 2. Greenland Ice Sheet Project 2 (GISP2) platinum (Pt) record compared to GISP2 cumulative concentrations of sea salt and continental dust. Concentrations of Cl, Ca, Na, Mg, and K are represented by stacked gray lines. The dotted black line is a lowess curve (50-y half-window) that shows data trends. Pt is shown on a semilog *Y*-axis for greater clarity. Results indicate that a peak in impact-related Pt (asterisk) coincides precisely with a peak at the onset of climate-related dustiness (plus sign), rising to an anomalous dust peak that is higher than ~99.7% of values in the previous 100,000 y. Data are from Mayewski et al. (1993) and Petaev et al. (2013).

NO_3, acetate, oxalate, and formate) taken from three ice cores: the GISP2, the Greenland Ice Core Project (GRIP), and the North Greenland Ice Core Project (NGRIP; fig. 1). We also investigated climatic and biomass-burning records from the Taylor Dome ice core and Taylor Glacier in Antarctica and from the Belukha ice core in Russia. These additional ice records were selected because they have sufficiently high chronological resolution to record detailed concentrations of multiple YD-age combustion aerosols.

GISP2 Ice Core. High-resolution data for NH_4 and $\delta^{18}O$ were independently acquired at a sampling resolution of ~3–5 y across the YD onset interval (Mayewski et al. 1993). This record for NH_4, a biomass-burning proxy, displays one of the highest peaks in the 120,000-y record in an interval dating to 12,830–12,828 cal BP (1712.3–1712.2 m; fig. 3*A*, 3*C*). This overlaps the Pt-rich interval dating to 12,836–12,815 cal BP (1712.250–1712.125 m) and coincides with the YD onset.

Before the onset of impact-related Pt deposition, the trendline of NH_4 values decreases, whereas after the onset of Pt deposition, NH_4 values abruptly increase and continue increasing for approximately a century (fig. 3*C*). This unusual ramp-up appears to indicate a long-term increase in wildfires, containing two of the highest NH_4 peaks in the entire record (fig. 3*C*), but such a century-long increase in biomass burning is not supported by the records for lake charcoal and AC/soot (Wolbach et al. 2018). In addition, it is unsupported by comparison to GISP2 Cl and Ca records, proxies for marine and continental dust, respectively. When NH_4 values are normalized to values of these two elements, the ramp-up nearly disappears (fig. A2), making its existence questionable; all original peaks remain, but with smaller amplitudes. The cause of this apparent ramp is unknown but may simply be an artifact of the increased windiness and/or other complex climatic changes related to the YD onset.

Nearly a dozen earlier NH_4 peaks are higher than that of the YD onset, as are several younger peaks that are likely related to increases in anthropogenic biomass burning (Cooke 1998; Power et al. 2008). The GISP2 NH_4 peak that coincides with the Pt anomaly is not the highest recorded, but it is greater than 99.96% of 26,535 measured NH_4 values, making it a standout in the entire pre-Holocene record.

Measurements for GISP2 $\delta^{18}O$, a proxy for atmospheric temperature, were at lower resolution (20-y

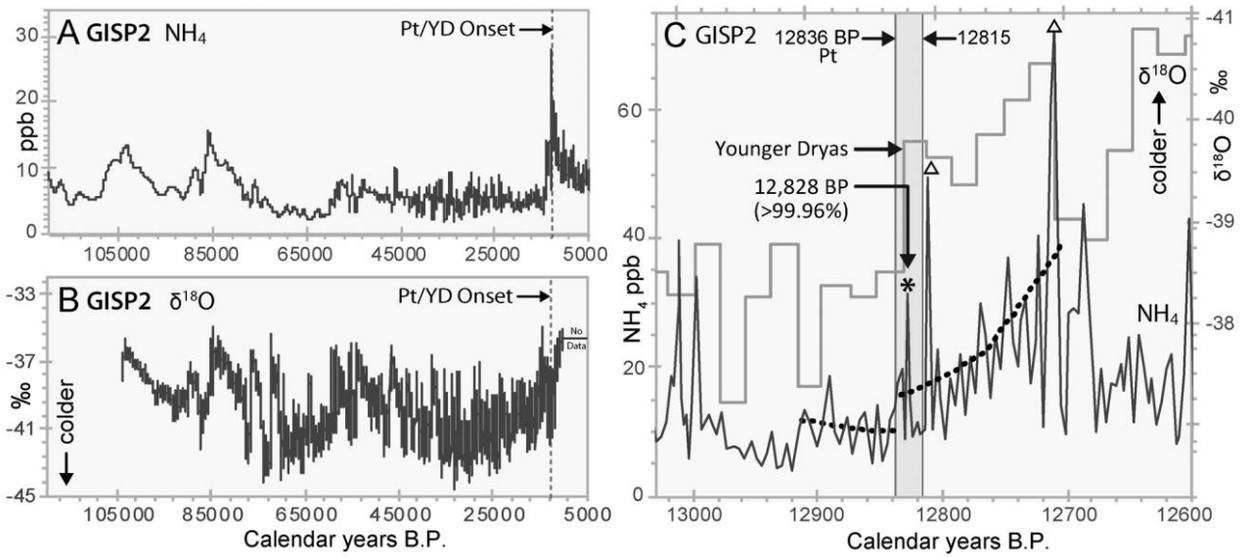

Figure 3. Greenland Ice Sheet Project 2 (GISP2) ice-core records. *A*, NH_4 record from 120,000 to 5000 cal BP. The most dramatic rise, culminating in the most robust peak, coincides with the Pt peak (dashed line). *B*, The $\delta^{18}O$ record from 120,000 to 5000 cal BP (lower values represent colder temperatures), exhibiting a major drop at the Younger Dryas (YD) onset. *C*, Pt anomaly from 12,836 to 12,815 cal BP (vertical gray bar); NH_4 measurements (solid black curve) between 13,050 and 12,600 cal BP; and $\delta^{18}O$ record (stair-step plot with lower values representing colder temperatures). Dotted lines are lowess curves, showing general trends in NH_4 values near the YD onset. A major NH_4 peak (asterisk) occurs at 12,828 cal BP, within the elevated-Pt interval. The shift in $\delta^{18}O$ values represent the onset of YD climate change, coinciding with both Pt and NH_4 peaks. NH_4 peaks marked with triangles are the two highest within the 120,000-y record; they occurred during an apparent ramp-up in biomass-burning activity beginning at the onset of anomalous Pt deposition. Site location is shown in figure A1 and data sources in table A4.

increments), but even so, the record clearly displays a dramatic shift to colder temperatures, marking the onset of the YD episode (fig. 3*B*, 3*C*; Stuiver et al. 1995). Most of this shift occurs across a single ice sample from ~1713.40 to ~1711.69 m, dating to 12,855–12,814 cal BP and overlapping the Pt anomaly.

Thus, four separate lines of evidence in the GISP2 core demonstrate that a series of highly anomalous changes co-occurred within a relatively thin ice section (1712.625–1712.000 m), spanning a mere 15 y between 12,836 and 12,821 cal BP (table 1). This demonstrates that the Pt anomaly (marking the YDB impact event; fig. 2) is synchronous with a peak in NH_4 concentrations (marking a major episode of biomass burning; fig. 3), an abrupt increase in dust concentrations (YD-related windiness reflecting a shift in atmospheric circulation), and a drop in $\delta^{18}O$ values (onset of the YD climatic cooling). This supports a strong interrelationship among all these processes.

NGRIP Ice Core. Fischer et al. (2015) independently measured NH_4 concentrations at annual resolution and attributed NH_4 peaks to biomass-burning activity across North America. They identified a single high NH_4 peak that begins at the YD onset, reflecting the largest biomass-burning episode from North American sources in the entire record. Fischer et al. (2015) also collected biomass-burning events into 201-y bins and found fewer apparent fires in the bin that includes the YD onset. However, if the YD cosmic impact produced just one major episode of biomass burning, we infer that multiple separate wildfires contributed to the overall episode, appearing as a single high NH_4 peak and thus obscuring the record.

The NGRIP ice interval from 120,000 to 5000 cal BP displays only one anomalously high peak in NH_4 (fig. 4*A*), and this is contemporaneous with the GISP2 Pt anomaly, as correlated with the GICC05 timescale (Rasmussen et al. 2008; Seierstad et al. 2014). This NH_4 peak occurs within a 3-cm interval centered on 1524.75 m, dating to 12,819 cal BP. This overlaps the GISP2 Pt anomaly's age range of ~12,836 to 12,815 cal BP. The amplitude of this peak is higher than 99.6% of the ~94,800 values measured in the entire record (fig. 4*A*). The NH_4 peaks at the YD onset in NGRIP correlate closely with those in GISP2, with an apparent age difference of only ~9 y, from 12,819 cal BP for NGRIP to 12,828 cal BP for GISP2. This small difference presumably is due to ice layer counting errors but is well within the GICC05 age uncertainty of ± 140 y, indicating statistical isochroneity.

The NGRIP NH_4 record also exhibits a ramp-up in values beginning at the YD onset, which on face value appears to mark a century-long episode of steadily increasing biomass burning, similar to that exhibited in the GISP2 record. At the end of the ramp, there is an NH_4 peak that is higher than 99.5% of all NH_4 values before the YD onset (fig. 4*C*), but, as discussed in the GISP2 results, when NH_4 values are normalized to Cl and Ca values, the existence of this ramp-up is questionable.

We also compiled and analyzed NGRIP values for $\delta^{18}O$, a proxy representing atmospheric temperature (fig. 4*C*; Steffensen et al. 2008). This proxy exhibits a major shift to colder temperatures, marking the onset of the YD, which occurred in a year or less between ~12,815 cal BP (1525.45 m) and ~12,814 cal BP (1525.42 m). This age span includes the end of the Pt anomaly in GISP2 (12,836–12,815 cal BP), indicating synchroneity between YD cooling in NGRIP and the Pt anomaly in GISP2.

GRIP Ice Core. Although the GRIP ice record extends to ~386,000 y, the data up to ~120,000 y old are considered more reliably dated. We compiled concentrations of the biomass-burning proxies NH_4, acetate, formate, and oxalate at relatively low chronological resolution of ~20–400 y/sample (fig. 5; Legrand et al. 1992; Fuhrer and Legrand 1997). Legrand et al. (2016) correlated NH_4 and formate, in particular, with known historical biomass burning in Canada, confirming that these proxies appear robust in reflecting biomass-burning activity in North America.

The GRIP concentrations of combustion aerosols began to increase sharply at ~12,816 cal BP, in the GICC05 cal BP timescale (bottom of sample: 1661.27 m), correlating with the GISP2 Pt anomaly (12,836–12,815 cal BP). Values rose to peaks less than 100 y later, at 12,710 cal BP (top of sample: 1657.725 m), closely correlating with the start of the peak in the GISP2 record of sea salt and continental dust. At the YD onset, GRIP NH_4 concen-

Table 1. Information on GISP2 Peak Proxies Analyzed

Proxy	Abbreviation	Significance	GISP2 depth (m)	Ages (cal BP)
Platinum	Pt	Cosmic impact	1712.625–1712.000	12,836–12,815
Dust	Cl, Ca, Na, Mg, K	YD wind strength	1712.70–1712.00	12,837–12,817
Ammonium peak	NH_4	Biomass burning	1712.30–1712.20	12,823–12,821
Oxygen isotope	$\delta^{18}O$	YD temperature	1713.40–1711.69	12,855–12,814

Note. GISP2 = Greenland Ice Sheet Project 2 core; YD = Younger Dryas.

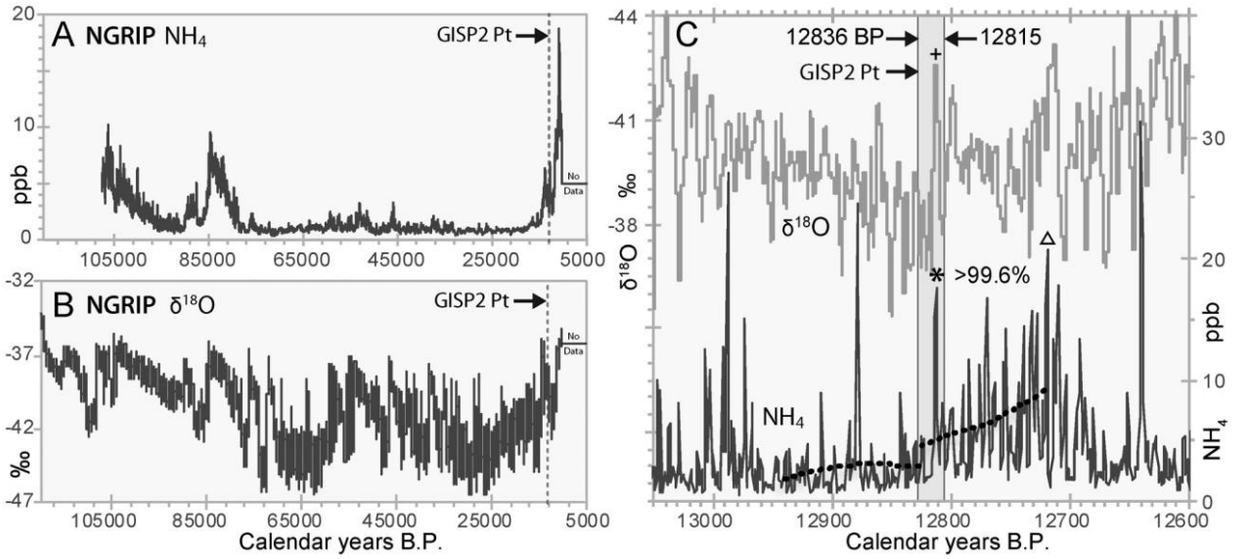

Figure 4. North Greenland Ice Core Project (NGRIP) ice-core records. *A*, NH_4 record from 120,000 to 5000 cal BP. One of the highest NH_4 peaks in the record coincides with the Greenland Ice Sheet Project 2 (GISP2) Pt peak (vertical dashed line, shown for reference). *B*, The $\delta^{18}O$ record from 120,000 to 5000 cal BP shows a major decrease in temperature at the Younger Dryas (YD) onset. *C*, Values for NH_4 (black curve) and $\delta^{18}O$ (gray stair-step curve) from 13,050 to 12,600 cal BP. The vertical gray bar denotes the GISP2 Pt anomaly interval, age-depth correlated between GISP2 and NGRIP with the Greenland Ice Core Chronology 2005 timescale. The thick dashed black lines are lowess curves for NH_4 values that show steady to declining values before the YD onset, followed by an apparent century-long ramp-up in NH_4 concentrations. A major NH_4 peak occurs at ~12,819 cal BP, within the span of anomalous Pt deposition. The $\delta^{18}O$ values show that the onset of YD cooling (marked with a plus sign) was contemporaneous with the NH_4 (asterisk) and Pt peaks. The two NH_4 peaks (asterisk and triangle) are higher than 99.6% of the values in the entire record. Site location is shown in figure 1 and data sources in table A4.

trations rose to their fourth-highest value, greater than 99.9% of all other values (fig. 5*A*). Simultaneously, concentrations of oxalate and formate reached their highest known concentrations in the ~386,000-y core (figs. 5*C*, 5*D*), with acetate abundances ranking among the highest in the entire core (fig. 5*B*). Also, the ratio between the NH_4 and formate at the YD onset in GRIP rose to its highest value, nearly 3 times as high as the nearest other value in the entire record (fig. 5*E*). These GRIP data reveal that YDB biomass burning represents the most anomalous episode of biomass burning in at least 120,000 y and possibly in the past ~386,000 y.

Antarctic and Siberian Ice Records. The Taylor Dome, Antarctica, ice-core record exhibits a small but distinct peak in NO_3 that closely correlates with the YD onset (fig. 6*A*; Mayewski et al. 1996). However, this peak is subdued relative to other NO_3 values for the Holocene and the record before 15,000 cal BP, but it is relatively much higher than that for the ice interval from 15,000 to 11,500 cal BP across the YD onset.

The base of the Belukha, Siberia, ice core exhibits a major peak in NO_3, indicating that a major episode of biomass burning occurred at the YD onset. Aizen et al. (2006) verified the link between NO_3 peaks in the Belukha core and biomass burning, on the basis of their observation of a NO_3 peak that is coeval with Siberian fires produced by the Tunguska impact in AD 1908.

Discussion

Significance of Combustion Aerosols. Well-dated high-resolution ice-core sequences are crucially important for providing records of biomass burning during the late Quaternary. Peaks in NH_4 are the most widely employed proxy for biomass burning in ice cores, strongly supported in some sequences by other combustion aerosols (Legrand et al. 1992; Mayewski et al. 1993). Several ice-core sequences (GISP2, NGRIP, GRIP, Taylor Dome, and Belukha) have revealed clear evidence that the onset of the YD is intimately associated with one of the highest and most pervasive late Quaternary peaks in each of NH_4, NO_3, formate, oxalate, and acetate. These peaks are effectively coeval with abrupt cooling and other climatic effects marking the onset of the YD episode.

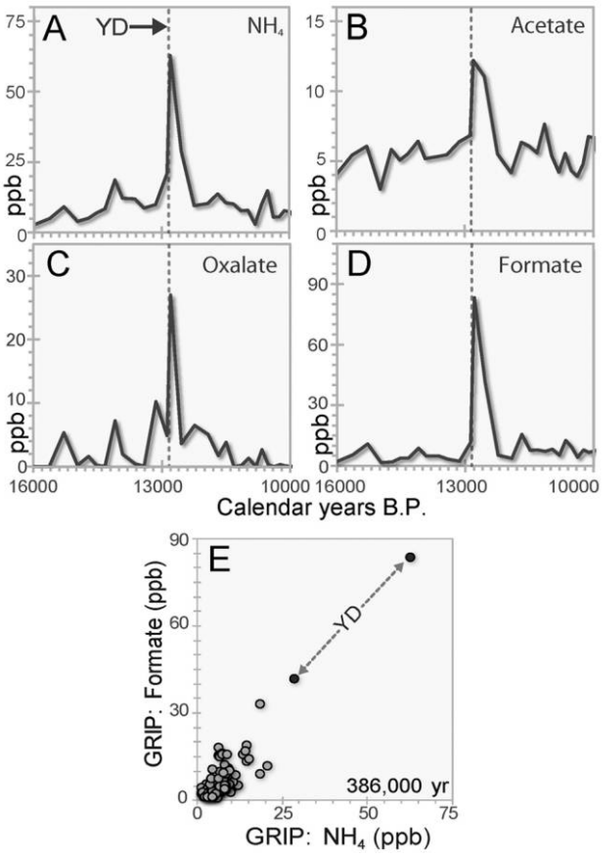

Figure 5. Combustion aerosols from Greenland Ice Core Project (GRIP) ice core. *A–D*, Coeval peaks in NH_4, acetate, oxalate, and formate, respectively, dating to or near the Younger Dryas (YD) onset and representing the highest or near-highest episode of biomass burning of the past 120,000–386,000-y record. *E*, Ratio of NH_4 to formate, two strong indicators of biomass burning. The two highest ratio values in the record comprise the single highest peak at the YD onset. Location of the GRIP site is shown in figure 1, and data sources are in table A4.

Another crucial factor involves atmospheric concentrations of CO_2, which are largely controlled by transfers between Earth's major carbon reservoirs (ocean and terrestrial biota), as well as carbon sinks (e.g., soils). CO_2 is produced during biomass-burning episodes that, if large enough, might be expected to affect atmospheric CO_2 concentration, such as during the biomass-burning peak at the YD onset. If so, an increase in atmospheric CO_2 should be apparent in polar ice. Although high-resolution ice-core records of CO_2 are not available from the Northern Hemisphere, Brook et al. (2015) reported atmospheric concentrations of CO_2 and $\delta^{13}C\text{-}CO_2$ from an ice sequence across the YDB interval in Taylor Glacier, Antarctica.

CO_2 values mostly increase before the YD onset, after which they exhibit a small, but abrupt, rise, followed by a gradual, long-term increase (fig. 7). Although degassing of the ocean to the atmosphere during deglaciation contributed to this generally rising pattern, the abrupt rise at the YD onset is consistent with a brief episode of major continental biomass burning. In addition, $\delta^{13}C\text{-}CO_2$ values decrease significantly and abruptly, beginning at the YD onset, and continue declining through the first ~500 y of the YD (fig. 7). This is consistent with a major loss of terrestrial carbon due to climate change, biomass burning during the early YD, and/or changes in ocean circulation.

The sudden cooling at the YD onset would have contributed to a major reduction in terrestrial biomass, but if ocean circulation and related climate changes were the only cause (Menviel et al. 2015), then the isotopic values of atmospheric CO_2 would not have rebounded as rapidly during the early YD. Because near-glacial conditions during the YD and related changes in ocean circulation persisted for much longer than 300 y (i.e., ~1300 y), it appears unlikely that the decline in $\delta^{13}C\text{-}CO_2$ was driven solely by the effects of climate and ocean circulation in reducing terrestrial biomass. In the absence of YDB biomass burning, the record suggests that YD cooling alone is unlikely to have accounted for the abruptness, magnitude (0.2‰), and brevity of the isotopic change.

The distinctive change in Antarctic $\delta^{13}C\text{-}CO_2$ after the YD onset provides further evidence for major transfer of organic carbon to the atmosphere. A number of processes could have caused this rise in $\delta^{13}C\text{-}CO_2$, including climate-related plant die-offs resulting in more fires as a result of increased fuel availability and/or an impact-related increase in wildfires consuming substantially more biomass over a brief interval. The sharp increase in CO_2, synchronous with the abrupt decrease in $\delta^{13}C\text{-}CO_2$, is limited to the earliest YD and hence is consistent with a rare episodic event.

The sudden rise in atmospheric CO_2 at the YD onset, recorded in Antarctic ice (fig. 7), is 2.44 ppm. Because each part per million is equivalent to 7.805 gigatons (Gt) of CO_2 in the global atmosphere (O'Hara 1990), the recorded rise corresponds to the release of 19.04 Gt of CO_2. Vegetation fires produce (~1.95–2.23) × 10^4 kg/ha of CO_2, not counting later reabsorption by new growth (Santín et al. 2016), so if the observed jump in CO_2 were due only to vegetation fires, it would be equivalent to the surface burning of (0.85–0.94) × 10^9 ha, or roughly 1 × 10^7 km^2. Because of lower sea levels at the time of the YD onset, the total land surface would have been somewhat larger than

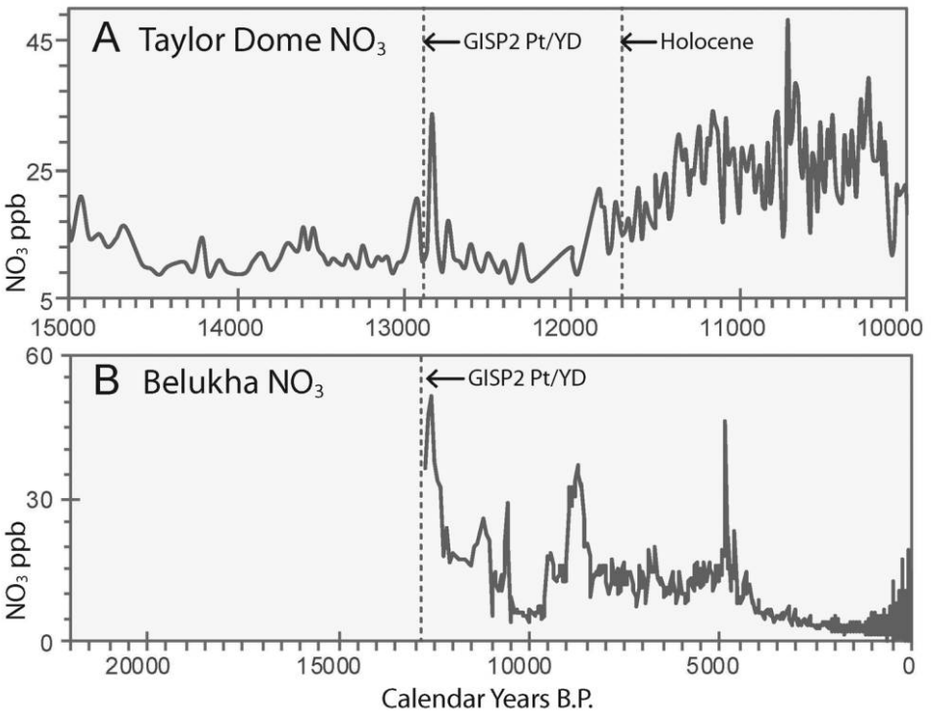

Figure 6. NO_3 concentrations in ice sections from Antarctica and Belukha, Siberia. *A*, Taylor Dome, Antarctica, ice-core abundances of NO_3, a biomass-burning proxy (Brook et al. 2015), age-correlated with the Greenland Ice Sheet Project 2 (GISP2) Pt peak and the Younger Dryas (YD) onset (vertical dashed line). *B*, NO_3 peak at the YD onset in the Belukha, Siberia, ice core, correlated by age with the GISP2 record. Ice deposition in the core began at the YD onset (dashed line). Locations are shown in figure 1 and data sources in table A4.

that today, at approximately 15×10^7 km^2, and so the burned percentage of global land surface would have been $(1 \times 10^7$ km$^2)/(15 \times 10^7$ km$^2)$, or approximately 6%. Still et al. (2003) estimated the area enclosing the contemporary global biomass to be 106.2×10^6 km^2; if that at the YD onset was similar, then ~9.4% of Earth's vegetated surface burned. This compares closely to calculations based on measured amounts of YDB AC/soot, suggesting that 5.0%–9.6% of biomass burned at the YD onset (Wolbach et al. 2018).

Significance of Widespread YDB Pt Peaks. The anomalously high Pt peak recorded at the onset of the YD in the GISP2 core (Petaev et al. 2013) and in widely distributed sedimentary sequences over North America (Moore et al. 2017) has been attributed to a major cosmic impact. Additional evidence presented here and in part 2 of this work (Wolbach et al. 2018) suggests that this cosmic impact also triggered widespread biomass burning that, in turn, contributed to "impact winter" and abrupt YD climate change (Firestone et al. 2007). On the other hand, Petaev et al. (2013) inferred no temporal, and hence casual, linkage between the YDB impact event and widespread biomass burning identified in the GISP2 core by Mayewski et al. (1993). However, that interpretation relied on two incompatible GISP2 timescales: a preliminary timescale in years before AD 1950 (Mayewski et al. 1993) and the Meese timescale in years before AD 2000 (Meese et al. 1997), a difference of 50 y. When all data sets are calibrated to the GICC05 timescale (cal BP; before AD 1950), the Pt anomaly, the biomass-burning peak, and the onset of YD climate change all co-occurred within the same 21-y ice interval and thus appear synchronous within the limits of ice-core dating.

Because anomalously high Pt concentrations also can result from other processes, including volcanism, it is important to consider nonimpact mechanisms. Both Firestone et al. (2007) and Moore et al. (2017) found no evidence of volcanic tephra in the Pt-rich YDB layer and or other strata. Furthermore, Moore et al. (2017) examined three samples of tephra from the Laacher See eruption in Germany, which occurred <200 y before the cosmic-impact event and potentially could have contaminated the YDB layer with volcanic Pt. However, they detected no measurable concentrations of Pt or magnetic spherules in that tephra.

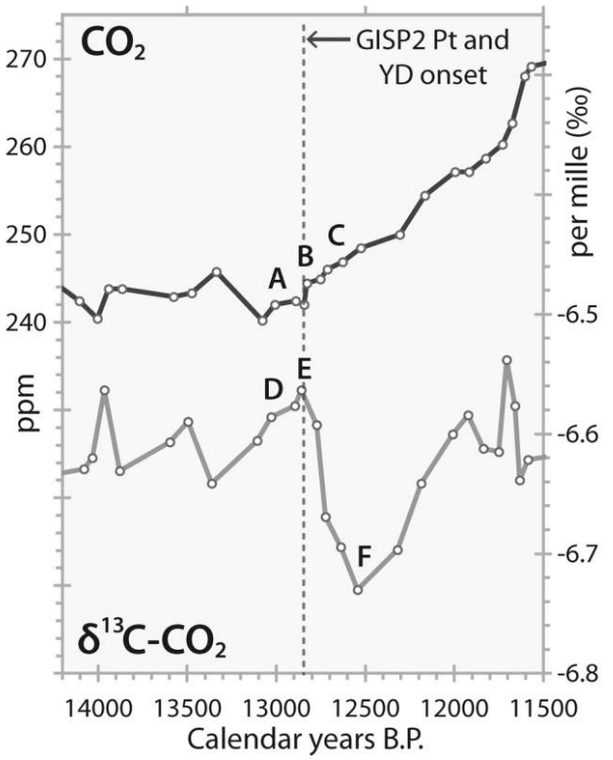

Figure 7. CO_2 and $\delta^{13}C$ concentrations over a 2800-y interval from Taylor Glacier, Antarctica. The dashed vertical line represents the Greenland Ice Sheet Project 2 (GISP2) Pt peak and the onset of Younger Dryas (YD) climate change as recorded in Greenland. CO_2 (upper line) was increasing immediately before the YD onset (A), rose sharply at the YD onset (B), and then increased steadily during the YD (C) until ~11,500 cal BP. The $\delta^{13}C$-CO_2 values (lower line) rose, gradually (D) peaking at the YD onset (E), declined sharply afterward (E–F), and suddenly rose again during the mid-YD, beginning at F. The sharp decline in $\delta^{13}C$-CO_2 in the earliest 300 y of the YD is consistent with a significant decrease in terrestrial carbon (organic degradation). Data are digitized from Brook et al. (2015).

Gabrielli et al. (2008) reported Pt concentrations in Greenland ice cores deposited by major eruptions from Mount Pinatubo, the largest in the twentieth century, and from Hekla volcano in Iceland. The maximum Pt enrichment they measured was 0.09 ppt; the Greenland ice concentrations at the YD onset found by Petaev et al. (2013) are nearly 1000 times higher, and the maximum YDB value measured by Andronikov et al. (2016*a*) is 5,000,000 times higher. For more information on YDB Pt, see "Widespread YDB Platinum Deposition" in the appendix.

In addition, GISP2 Pt concentrations (Petaev et al. 2013) can be compared with the GISP2 sulfate record, a proxy for volcanic eruptions (Mayewski et al. 1993). This reveals that although three major volcanic eruptions occurred near the YD onset (fig. 8), no significant Pt peaks are associated with any episode of volcanism recorded in this core. These various lines of evidence, therefore, suggest that volcanism is an unlikely source for the YDB Pt anomaly.

The average Pt/Ir ratio for the upper continental crust is ~1 (Rudnick and Gao 2003), whereas meteoritic ratios are typically much higher, averaging 42 (ratio range: 13,500–0.1; GERM Reservoir Database 2016). In the GISP2 ice core, Petaev et al. (2013) measured a maximum Pt/Ir ratio of ~500, similar to those of some iron meteorites, and thus concluded that an iron meteorite was the likely source of YDB Pt deposition. However, Andronikov et al. (2016*a*) reported much lower average Pt/Ir ratios of 42 (range: 91–12) in YDB magnetic spherules that do not require an iron meteorite as source.

To help determine the potential type of YDB impactor, we investigated Pt-to-palladium (Pt/Pd) ratios and Pt-to-iridium (Pt/Ir) ratios. Elemental abundances of YDB Pt, Pd, and Ir are available from eight sites (Firestone et al. 2007; Moore et al. 2017), excluding Greenland, where Pd measurements are not available. The YDB Pt/Ir ratios average 7.8 (range:

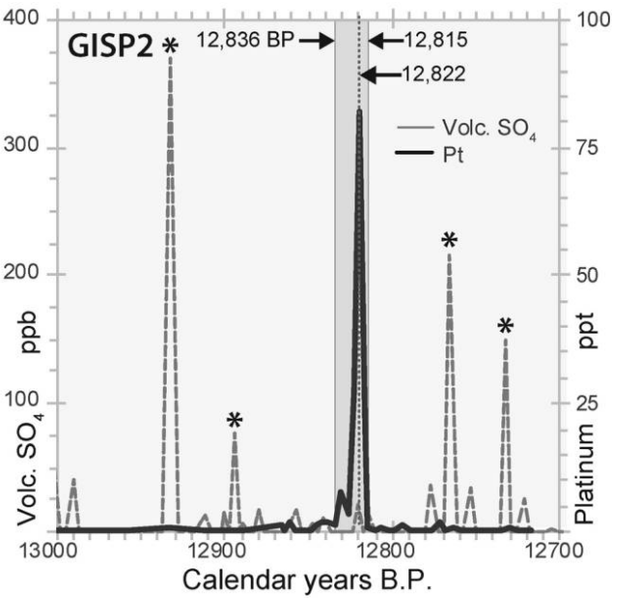

Figure 8. Greenland Ice Sheet Project 2 (GISP2) platinum (Pt) and volcanic sulfate (Volc. SO_4). Pt (ppt) deposition is represented by the black curve, and sulfate (ppb) is represented by the dashed curve. The vertical gray bar represents the GISP2 Pt anomaly, dating from 12,836–12,815 cal BP, with a high peak centered at 12,822 cal BP (dotted vertical line). None of the four highest volcanic sulfate peaks (asterisks) corresponds to the Pt anomaly.

3.8–0.1), and YDB Pt/Pd ratios average 1.5 (range: 3.4–0.7), both of which are higher than the average crustal ratios. We compared YDB ratios to those from five types of meteorites (fig. 9*A*; GERM Reservoir Database 2016) and found that the ratios from three YDB sites appear lower than meteoritic values. However, ratios for the other five agree with the ratios of iron meteorites ($n = 10$) but also overlap ratios from some achondrites ($n = 19$), chondrites ($n = 47$), Martian meteorites ($n = 6$), and/or ureilites ($n = 23$). These data suggest that YDB Pt concentrations most likely do not result from any single type of meteorite.

We also compared the same YDB ratios of Pt, Pd, and Ir with those of three groups of impactites, which are rocks that have been melted through cosmic impact and thus contain small quantities of impactor material. We used impactite data from the GERM Reservoir Database (2016) for the 66 Ma K-Pg impact event ($n = 60$), a 145 Ma impact ($n = 8$), and a 2.55 Ga impact ($n = 18$). For three YDB sites, Pt/Pd and Pt/Ir ratios are higher than those for these three groups of impactites, and ratios from the other five YDB sites overlap or are close to ratios of known impactites (fig. 9*B*). These data suggest that YDB Pt concentrations could result from the impact-related mixing of meteoritic material and terrestrial target rocks.

Although the above analyses indicate that the YDB impactor could have been any one of several types of meteorite, the wide range of YDB Pt/Ir ratios (12–1264) is inconsistent with collision with a single type of meteorite. Comets are a compositionally variable mix of volatile ices, meteoritic material, and presolar dust (Flynn et al. 2006), and although available samples of cometary material are too small to allow measurements of Pt, Pd, and Ir, other elemental ratios are available from Comet Wild 2 (Flynn et al. 2006). Iron-to-nickel (Fe/Ni) ratios range widely from 7 to 286, and chromium-to-copper (Cr/Cu) ratios range from 0.05 to 285 (Flynn et al. 2006), similar to the wide range of YDB Pt/Ir ratios (12–1264). These wide ranges of elemental ratios confirm that cometary material is heterogeneous, similar to the YDB samples. Although the type of YDB impactor remains unclear, the current evidence does not support any specific meteoritic type as source. Instead, the broad extent of biomass burning at the YD onset is more consistent with Earth's collision with a fragmented comet that in turn, triggered widespread wildfires.

Astronomical Hypothesis for the YDB Impact Event. Regarding the probability of a swarm of cometary fragments hitting the Earth, Boslough et al. (2013) claimed that the YDB event is "statistically and physically impossible," whereas Napier et al. (2013) argued that such an encounter in the late Quaternary is a "reasonably probable event." We outline the latter hypothesis below; details and prime references are given in Napier (2015).

With currently accepted impact rates, there is an expectation of one extraterrestrial impact of energy 100–200 megatons over the past 20,000 y, which is inadequate to produce the observed global trauma (Bland and Artemieva 2006). However, near-Earth

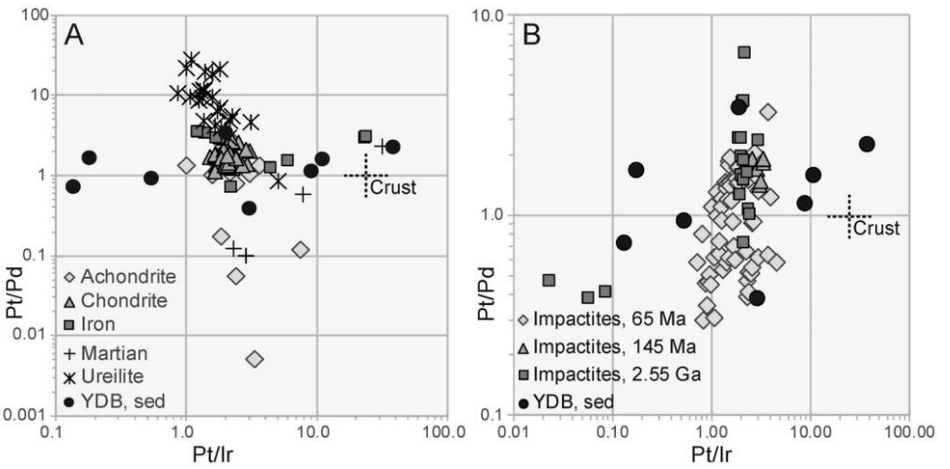

Figure 9. Ratios of platinum to palladium (Pt/Pd) and platinum to iridium (Pt/Ir) for rocks, sediments, and meteorites. Younger Dryas boundary (YDB) sites are represented by filled circles. Dashed crosses represent upper crustal abundances. *A*, Elemental ratios for eight YDB sites plotted against those for five types of meteorites. Five of the 8 sites overlap or show close correspondence to meteoritic compositions. *B*, Elemental ratios for eight YDB sites plotted against those for impactites produced by three impact events. Five of the 8 YDB sites overlap or closely correspond to impactite compositions.

surveys of hazardous interplanetary objects are limited to the past ~30 y, and extrapolation of contemporary impact rates to timescales beyond 10^4 y cannot be justified without further investigation, especially for comet populations.

Comets entering Earth-crossing orbits, which are thus potential collision hazards, may be long-period (LP) objects (200 ky $\lesssim P \lesssim$4 My), Halley-type (HT; 20 y $\lesssim P \lesssim$ 200 y), Jupiter family (JF)–type (4 y $\lesssim P \lesssim$ 20 y), or Encke-type ($P \lesssim$ 4 y), the latter currently with a population of 1. The LP system is spherical, containing as many comets in retrograde orbits as in prograde, and derives from the Oort cloud. The HT system is spheroidal, with a preponderance of comets in direct orbits, while the JF and Encke comets are in direct orbits close to the plane of the ecliptic. There may be ~100 active comets with diameters over 2.3 km in the HT population and ~450 in the JF system, although these numbers are very uncertain. Both these populations are evanescent, with a typical JF comet surviving for only 200–300 revolutions (~3000 y) before disintegration is complete. To maintain a steady state, new comets must enter the JF system about once a decade and the HT system about once every century. The likely replacement reservoirs are the Oort cloud and a trans-Neptunian population of icy bodies on the fringes of the planetary system, the latter of which was largely unknown 25 y ago. Its properties are still being explored, but it is estimated to contain 8 billion comets more than 1 km in diameter; the Oort cloud may contain a trillion comets.

Dormant comets, called "centaurs," have been detected in transition from these reservoirs to the JF population. They are in unstable orbits crossing those of Jupiter, Saturn, and Uranus, becoming more unstable as they move inward and becoming active when they cross the water-snow line at ~2.9 astronomical units (au) from the Sun (1 au = the mean Earth-Sun distance). The archetypal centaur, Chiron, currently orbits between Saturn and Uranus. Its half-life for ejection from the solar system is about 1 My, and that for evolution into a Jupiter-crossing orbit is 0.1–0.2 My (Hahn and Bailey 1990). Population-balance arguments indicate that at any given time there may be four to seven centaurs larger than 240-km-wide Chiron inside 18 au and about 30 that are >100 km in diameter. Their orbits are chaotic and can be followed only statistically, because small changes in initial conditions induce large subsequent variations (the butterfly effect). Eventually, about half the centaurs in Chiron-like orbits become Jupiter crossers at some point, and a tenth become Earth crossers, moving in and out of Earth-crossing epochs repeatedly (fig. 10).

The mass distribution of centaurs is top-heavy, and the replenishment of the JF and comets in Encke-like orbits is erratic, with occasional large injections of mass into the inner planetary system. A 250-km comet with typical density 0.5 g/cm^3 has 2000 times the current mass of the JF and 1000 times that of the entire current near-Earth asteroid system. In terms of terrestrial interactions, its disintegration prod-

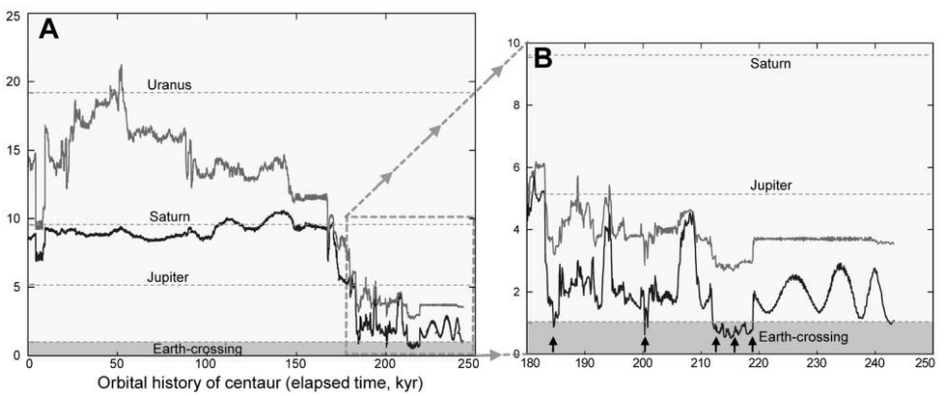

Figure 10. Computer-modeled orbital evolution of a Chiron clone. Simulation indicates that the clone eventually becomes Earth crossing (gray boxed area below horizontal dashed "Earth" line). Light gray curves represent semimajor axes (half of the longest orbital axis) and black curves the perihelion (the orbital point closest to the Sun). *A*, The Chiron-clone centaur, orbiting originally in the Saturn/Uranus region, moves into Earth-crossing orbit (gray boxed area below horizontal dashed "Earth" line) after 180 ka. *B*, Enlarged orbital history from 180 to 250 ka, showing that once a centaur enters an Earth-crossing epoch (gray boxed area below horizontal dashed "Earth" line), it does so repeatedly as its orbit fluctuates (black arrows mark Earth-crossing episodes). The Chiron clone is typically destroyed in a cascading series of fragmentations, and its physical lifetime is likely to be much shorter than the dynamical lifetimes indicated.

ucts, during its active lifetime, will thus greatly dominate over those of the near-Earth asteroids. For a 100-km comet, the factors are 128 and 64, respectively. The timescale for an enhancement in mass of the near-Earth environment is ~0.5 My for a factor 1000 and ~0.03–0.1 My for a factor 100.

The main modes of disintegration of a comet are sublimation and fragmentation. The latter has two prime modes: tidal splitting, in which the comet breaks into fragments after a close planetary or solar encounter, and spontaneous splitting, in which the main nucleus stays intact while a number of short-lived cometary fragments split off, often disappearing from sight after a few weeks or days.

Fragmentation is the major mode of comet disintegration: the total mass lost by small fragments repeatedly spalling from the nucleus may be comparable to the mass of the nucleus itself (Boehnhardt 2004). A 100-km comet of mass 2.5×10^{20} g, with perihelion of ~0.34 au, loses typically $\sim 10^{16}$ g of material through sublimation during each perihelion passage, but $\sim 10^{17}$–10^{18} g during a splitting event, equivalent in mass to $\sim 10^{7}$–10^{8} Tunguska bolides. Such an event may happen anywhere along its orbit. For a comet in an Encke-like orbit, such fragmentations are expected every third or fourth orbit (di Sisto et al. 2009). These splittings may occur anywhere but have a tendency to occur near perihelion. Debris from disintegrating comets readily spreads out to cross sections much greater than Earth's diameter and so is encountered more frequently, as can be seen by the prevalence of meteor showers in the night sky, the products of cometary decay. During dormant phases, in which sublimation decreases, an active comet becomes more asteroidal in appearance through acquiring a mantle of dust and heavy organics. These phases may persist for up to 40% of the lifetime of the comet.

The structure of the meteoroid population in the inner planetary system has been determined both through numerous individual studies of meteors, going back to the 1950s, and from recent large-scale radar and optical surveys. As many as 100 meteor showers are accepted by the International Astronomical Union, but a total of 230 showers and shower components have now been identified from video-based meteoroid orbit surveys (Wiegert et al. 2009; Jenniskens et al. 2016). Some of these streams are multicomponent, indicating that they result from cascades of disruption of a parent body into subcomponents.

A prominent feature of this orbiting material is an interrelated system of meteoroidal material called the Taurid Complex. At least 20 observed streams are embedded within it, with the meteoroids moving in low-inclination, short-period, Earth-crossing orbits. Many of these streams contain bodies of kilometer and subkilometer dimensions, including the 4.8-km-wide Comet Encke. A limitation of meteor surveys is that they detect only material that hits Earth. It is therefore possible that the number of meteoroid streams associated with the progenitor of the Taurid Complex is greater than the ~20 that have been observed. A dust trail along the orbit of Encke has also been detected, with a lower mass limit of 7 million tons inferred from the Spitzer infrared space telescope (Reach et al. 2007). This trail, which is well away from Earth intersection, extends around the entire orbit and would disperse in some revolutions. Such trails, distinct from comet tails, are a generic feature of short-period comets.

The Taurid Complex is best explained as debris from the breakup of a large comet (~100 km) in a short-period, Earth-crossing orbit that recently arrived from the centaur system (Clube and Napier 1984; Steel and Asher 1996). The orbits of the meteor streams and their associated bodies precess and disperse because of the influence of Jupiter and Saturn. From the observed dispersal of the Taurids, Steel and Asher (1996) concluded that the progenitor comet was at least 20,000–30,000 y old. Comet Encke, part of the Taurid Complex, never approaches closer than 26,000,000 km from Earth at present.

The fragments of a splitting event disperse as they move away from the comet. Recently released cometary material forms an elongated, dense trail typically a few hundred Earth radii long and 10 radii wide within an orbit (Napier 2015; Napier et al. 2015). Taking account of orbital precession and nutation, the recurrence time of encounters between Earth and one such debris swarm in an Encke-like orbit is $\tau \sim 500/\sigma$ My, where the effective cross-sectional area σ of the swarm is in Earth radii. If there is an average of one such swarm at any time, we expect passage through it about once in 50,000 y, in the course of which the Earth will encounter $10^{17}/\sigma \sim 10^{13}$–$10^{14}$ g of material over a few hours, entering the Earth's atmosphere at 30 km/s. The debris so encountered will generally be a mixture of dust and larger fragments, energetically equivalent to the impact of ~1000–10,000 Tunguskas and with the potential to create severe biotic and climatic disturbances (Hoyle and Wickramasinghe 1978).

The presence of multiple meteor streams within the Taurid Complex, including "asteroids" orbiting within them, indicates that the original comet evolved via a cascading hierarchy of fragmentations. Over its active lifetime, the original comet and its offspring may have generated several thousand trails of mass $\sim 10^{15}$–(2×10^{17}) g, spreading and dispersing

over time, containing subkilometer bodies that continued to generate meteoroid streams as they disintegrated.

Asher and Clube (1993) demonstrated theoretically that the 7:2 mean motion resonance with Jupiter plays an important role in shepherding Taurid meteoroids, building up a swarm of enhanced density over a timescale of 1000 y. The existence of this swarm has been confirmed through epochs of enhanced fireball activity going back ~60 y (Asher and Clube 1993; Dubietis and Arlt 2007; Reach et al. 2007) and possibly through Far Eastern historical records going back a thousand years (Hasegawa 1992). More meteoroids struck the Moon over five days in 1975, during a passage through the daytime Taurids, than over the five years of the lunar seismic record. Thus, over the late Quaternary lifetime of this exceptionally large short-period, Earth-crossing comet, one or more encounters with a swarm of bolides whose aggregate kinetic energy is comparable to that of a nuclear war is a "reasonably probable event" (Napier et al. 2013).

Firestorms from Encounters with Comet Swarms. Although the blast damage from the Tunguska impact covered 2000 km^2, the area of forest that was ignited was only a tenth of that (Florenskiy 1965). Conditions in the Siberian taiga of the twentieth century may not, however, extrapolate reliably to Earth's Northern Hemisphere ~12,800 y ago. The radiant energy of a megaton-class nuclear explosion unfolds over a few seconds, comparable to that from a Tunguska-type event, and the effects of an airburst are probably similar for both types of energy release. Therefore, we may use studies of wildfires following a nuclear war (e.g., Crutzen et al. 1984; National Research Council 1985; Mills et al. 2014) as rough guides to the consequences of multiple impacts. Crutzen et al. (1984) quote minimum forest fire areas of 500, 1000, and 2100 km^2 following 1-, 3-, and 10-megaton explosions, respectively, while the maximum spread areas quoted by Hill (1961) are about a factor of 10 higher.

The ignition threshold for wood is about 4×10^8 $ergs/cm^2$, applied for 1–20 s. If the burn area required to produce the increase in soot and charcoal measured at the YDB is 10^7 km^2 (eq. [3] in Wolbach et al. 2018), then an energy input of $\sim 4 \times 10^{25}$ ergs is required, that is, about 10^3 megatons. Assuming that three-quarters of the external input does not directly affect flammable areas of Earth, then approximately four times this energy is required to produce wildfires, possibly reduced by a factor of a few times (Hill 1961). This equals the kinetic energy of 10^{13} g of material entering the Earth's atmosphere at the entry speed of Taurid material (30 km/s).

The best explanation for the available evidence is that Earth collided with a fragmented comet. If so, aerial detonations or ground impacts by numerous relatively small cometary fragments, widely dispersed across several continents, most likely ignited the widespread biomass burning observed at the YD onset.

Atmospheric Effects. The environmental effects of (5×10^{12})–10^{14} g of smoke injected into the atmosphere have been extensively discussed in a nuclear-winter context (Crutzen et al. 1984; National Research Council 1985; Mills et al. 2014) and include multidecadal cooling even with the lower mass input. In the case of passage through a dense cometary tail, there is the additional factor of 10^{13}–10^{14} g of meteoric material trickling down through the stratosphere, much of which would be converted to submicron smoke with a high optical-scattering coefficient (Klekociuk et al. 2005) and a long residence time, significantly darkening the sky, with probable climatic effects (Hoyle and Wickramasinghe 1978; Napier 2015). The cooling of the upper atmosphere due to the diminution of vertical transport of water might create supercooled crystals in the high atmosphere. These have high reflectivity and could lead to a self-sustaining, high-albedo layer of ice crystals in the stratosphere (Hoyle 1981). Long-lived oceanic cooling and the regrowth of sea ice and ice caps also would be expected (Mills et al. 2014).

The onset of the YD was clearly an exceptional event, and the contemporaneous Taurid progenitor comet was also exceptional, in terms of both its size and its Earth-crossing configuration. Its fragmentation history over the late Quaternary could plausibly have resulted in a brief, violent hurricane of bolides capable of generating the extensive wildfires and depositing impact-related proxies observed in the YDB layer.

Impact-Related Ozone Depletion. Large impactors are expected to cause depletion of stratospheric ozone (O_3), which, in turn, triggers an increase in solar irradiance reaching Earth's surface in the ultraviolet spectrum (UV-B; 280–315-nm wavelength). Impact-induced UV-B levels are predicted to far exceed those currently experienced (Pierazzo et al. 2010). Ultraviolet-B radiation has significant biological effects, including sunburn, skin cancer, cataracts for humans and other animals, and reductions in growth and productivity in plants (both terrestrial and aquatic). Pierazzo et al. (2010) modeled the changes in atmospheric chemistry associated with impactors and found that a 1-km impactor, having 2.23×10^{27} ergs of kinetic energy, would cause a >70% reduction in the column density of O_3 at mid-to-high latitudes for >2 y. Melott et al. (2010) estimated an impactor energy of 4×10^{29} ergs for the YDB, so we

consider Pierazzo et al.'s (2010) result to be a lower limit for YDB O_3 depletion. While Pierazzo et al. (2010) discussed some potential impacts following this level of O_3 depletion, they included only numerical estimates of the UV index (a proxy for skin damage in humans) and erythemal (sunburn) irradiance. Thomas et al. (2015) examined a wide range of biological effects associated with O_3 depletion of similar magnitude (~70%) and found that it would increase the risk of human skin cancer by a factor of ~13 and inhibit the growth of oat seedlings fivefold. In addition, changes in the productivity of aquatic phytoplankton species would range from a few percent (Neale and Thomas 2016) to more than a factor of 5.

The likely presence of atmospheric particulates and aerosols can reduce UV-B irradiance reaching the ground. However, Thomas et al. (2016) found that changes in O_3 column density were more important than increases in aerosol optical depth and that high optical depth is expected to last only for months, while significant O_3 depletion could persist for several years. Therefore, it is reasonable to conclude that depletion of O_3 after an impact would have significant deleterious effects on ecosystems through direct damage to primary plant producers, humans, and many other animals.

Expanded YDB Impact Theory. On the basis of evidence from the YDB, known impact events, and nuclear detonations, here we update the YDB impact theory.

A giant, ≥100-km-diameter comet entered an Earth-crossing orbit in the inner solar system and began a cascade of disintegrations (Napier 2010). Numerous cometary fragments from the debris stream entered Earth's atmosphere ~12,800 y ago and detonated above and/or collided with land, ice sheets, and oceans across at least four continents in the Northern and Southern Hemispheres (Firestone et al. 2007; Napier 2010). Vaporization of cometary materials and platinum-group element (PGE)–rich target rocks injected Pt, Ir, Os, and other heavy metals into the stratosphere (Petaev et al. 2013; Wu et al. 2013; Moore et al. 2017), accompanied by impact-related nanodiamonds (Kinzie et al. 2014), meltglass (Bunch et al. 2012), and microspherules (for all proxies, see table A3). The impact event destabilized the ice-sheet margins, causing extensive iceberg calving into the Arctic and North Atlantic Oceans (Bond and Lotti 1995; Kennett et al. 2018). The airburst/impacts collapsed multiple ice dams of proglacial lakes along the ice-sheet margins, producing extensive meltwater flooding into the Arctic and North Atlantic Oceans (Teller 2013; see Kennett et al. 2018 for summary and references). Destabilization of the ice sheet also may have triggered extensive subglacial ice-sheet flooding, leaving widespread, flood-related landforms across large parts of Canada (Shaw 2002). The massive outflow of proglacial lake waters, ice-sheet meltwater, and icebergs into the Arctic and North Atlantic Oceans caused rerouting of oceanic thermohaline circulation. Through climatic feedbacks, this, in turn, led to the YD cool episode (Broecker 1997; Teller 2013; Kennett et al. 2018). Unlike for typical warm-to-cold climate transitions, global sea levels rose up to 2–4 m within a few decades or less at the YD onset, as recorded in coral reefs in the Atlantic and Pacific Oceans (Bard et al. 2010; Kennett et al. 2018). Multiple impact-related drivers caused warm interglacial temperatures to abruptly fall to cold, near-glacial levels within less than a year (Steffensen et al. 2008), possibly in as little as 3 mo (Manchester and Patterson 2008). A rapid increase in wind strength across Greenland at the YD onset deposited extensive dust, sea salt, Pt-rich impact debris, and combustion aerosols into the ice sheet (this study). The radiant and thermal energy from multiple explosions triggered wildfires that burned ~10% of the planet's biomass, producing charcoal peaks in lake/marine cores that are among the highest in 368,000 y (Wolbach et al. 2018). This widespread biomass burning generated large amounts of long-lived, persistent AC/soot that blocked nearly all sunlight, rapidly triggering impact winter that transitioned into the YD cool episode (Wolbach et al. 2018). This widespread biomass burning delivered combustion aerosols (e.g., NH_4 and NO_3) to Greenland ice at some of the highest concentrations in ~120,000–386,000 y (this study). NH_4, NO_3, and other biomass-burning by-products underwent chemical reactions in the atmosphere that resulted in acid rain (Firestone et al. 2007; this study). Climate change, wildfires, and related environmental degradation contributed to the late Pleistocene megafaunal extinctions and human cultural shifts and population declines (Firestone et al. 2007; Anderson et al. 2011; Wolbach et al. 2018; this study).

Conclusions

From ice-sheet and ice-core records in Greenland, Antarctica, and Russia, the evidence reported in this study supports the co-occurrence of (1) the YDB impact event, represented by elevated Pt concentrations and many other impact-related proxies; (2) the YD cool episode, represented by a temperature decrease reflected by changes in $\delta^{18}O$ and elevated concentrations of Cl, Ca, Na, Mg, and K, reflecting increased atmospheric dustiness and changes in atmospheric circulation; and (3) a major episode of biomass burning, represented by anomalously high coeval peaks in NH_4, NO_3, acetate, oxalate, and formate. For the

GISP2 core, all of these proxies overlap in the same Pt-enriched, 21-y-long section of ice that peaks at 12,822 cal BP (range: 12,836–12,815 cal BP), a span that overlaps the Bayesian-calculated age for the YDB impact event of 12,835–12,735 cal BP (Kennett et al. 2015). Multiple lines of ice-core evidence appear synchronous, and this synchroneity of multiple events makes the YD interval one of the most unusual climate episodes in the entire Quaternary record. Because a cosmic impact is the only known event capable of simultaneously producing the collective evidence discussed in the two parts of this study, a cause-and-effect relationship among these events is supported, as proposed by YDB theory.

Author Affiliations

1. Department of Chemistry, DePaul University, Chicago, Illinois 60614, USA; 2. Department of Geography, University of Tennessee, Knoxville, Tennessee 37996-0925, USA; 3. Climate Change Institute, University of Maine, Orono, Maine 04469, USA; 4. Department of Natural Sciences, Elizabeth City State University, Elizabeth City, North Carolina 27909, USA; 5. Geology Program, School of Earth Science and Environmental Sustainability, Northern Arizona University, Flagstaff, Arizona 86011, USA; 6. Department of Nuclear Engineering, University of California, Berkeley, California 94720, USA; 7. Restoration Systems, Raleigh, North Carolina 27604, USA; 8. Instituto de Investigaciones en Ciencias de la Tierra, Universidad Michoacana de San Nicolás de Hidalgo, Morelia, Michoacán, Mexico; 9. Santa Barbara Museum of Natural History, Santa Barbara, California 93105, USA; 10. Kimstar Research, Fayetteville, North Carolina 28312, USA; 11. Faculty of Science, Charles University, Prague, Czech Republic; Institute of Geology, Czech Academy of Science of the Czech Republic, Prague, Czech Republic; and University of Alaska, 903 Koyukuk Drive, Fairbanks, Alaska 99775, USA; 12. Center of Excellence in Remote Sensing Education and Research, Elizabeth City State University, Elizabeth City, North Carolina 27909, USA; 13. Quaternary Surveys, 26 Thornhill Avenue, Thornhill, Ontario L4J 1J4, Canada; 14. Department of Physics and Astronomy, University of Kansas, Lawrence, Kansas 66045, USA; 15. Department of Geological Sciences, East Carolina University, Greenville, North Carolina 27858, USA; 16. Savannah River Archaeological Research Program, South Carolina Institute of Archaeology and Anthropology, University of South Carolina, New Ellenton, South Carolina 29809, USA; 17. Buckingham Centre for Astrobiology, University of Buckingham, Buckingham MK18 1EG, United Kingdom; 18. Comet Research Group, Dewey, Arizona 86327, USA; 19. Department of Anthropology and Department of Geology, University of Cincinnati, Cincinnati, Ohio 45221, USA; 20. Department of Physics and Astronomy, Washburn University, Topeka, Kansas 66621, USA; 21. Department of Earth Science and Marine Science Institute, University of California, Santa Barbara, California 93106, USA.

ACKNOWLEDGMENTS

B. Culleton (Pennsylvania State University) provided essential assistance with ^{14}C calibration and OxCal, along with C. Bronk Ramsey (University of Oxford). S. Horn and M. Valente (University of Tennessee) offered valuable suggestions for improving the manuscript. G. Kletetschka was supported by the Czech Science Foundation (GACR 17-05935S) and institutional grant RVO 67985831. J. P. Kennett appreciates long-term support from the US National Science Foundation (Marine Geology and Geophysics) and also support from a Faculty Senate grant of the University of California, Santa Barbara. H. Kloosterman (now deceased) assisted with European sites. P. Bobek and H. S. Svitavska assisted at the Stara Jimka site in the Czech Republic. A. L. Melott and B. C. Thomas are grateful for support from National Aeronautics and Space Administration Exobiology and Evolutionary Biology grant NNX14AK22G. We acknowledge the valuable contributions of coauthor David Kimbel, who passed away during the writing of the manuscript. Finally, we thank the editor of the *Journal of Geology*, several anonymous reviewers, and reviewer J. Hagstrum, all of whom generously and thoughtfully contributed to improving the manuscript.

REFERENCES CITED

Adatte, T.; Keller, G.; Stüben, D.; Harting, M.; Kramar, U.; Stinnesbeck, W.; Abramovich, S.; and Benjamini, C. 2005. Late Maastrichtian and K/T paleoenvironment of the eastern Tethys (Israel): mineralogy, trace and platinum group elements, biostratigraphy and faunal turnovers. Bull. Soc. Geol. Fr. 176:37–55.

Aizen, V. B.; Aizen, E. M.; Joswiak, D. R.; Fujita, K.; Takeuchi, N.; and Nikitin, S. A. 2006. Climatic and

atmospheric circulation pattern variability from ice-core isotope/geochemistry records (Altai, Tien Shan and Tibet). Ann. Glaciol. 43:49–60.

Anderson, D. G.; Goodyear, A. C.; Kennett, J. P.; and West, A. 2011. Multiple lines of evidence for possible human population decline/settlement reorganization during the early Younger Dryas. Quat. Int. 242: 570–583.

Andronikov, A. V., and Andronikova, I. E. 2016. Sediments from around the lower Younger Dryas boundary (SE Arizona, USA): implications from LA-ICP-MS multi-element analysis. Geogr. Ann. Ser. A Phys. Geogr. 98:221–236. doi:10.1111/geoa.12132.

Andronikov, A. V.; Andronikova, I. E.; Loehn, C. W.; Lafuente, B.; Ballenger, J. A.; Crawford, G. T.; and Lauretta, D. S. 2016*a*. Implications from chemical, structural and mineralogical studies of magnetic microspherules from around the lower Younger Dryas boundary (New Mexico, USA). Geogr. Ann. Ser. A Phys. Geogr. 98:39–59.

Andronikov, A. V.; Rudnickaitė, E.; Lauretta, D. S.; Andronikova, I. E.; Kaminskas, D.; Šinkūnas, P.; and Melešytė, M. 2015. Geochemical evidence of the presence of volcanic and meteoritic materials in late Pleistocene lake sediments of Lithuania. Quat. Int. 386:18–29.

Andronikov, A. V.; Subetto, D. A.; Lauretta, D. S.; Andronikova, I. E.; Drosenko, D. A.; Kuznetsov, D. D.; Sapelko, T. V.; and Syrykh, L. S. 2014. In search for fingerprints of an extraterrestrial event: trace element characteristics of sediments from the lake Medvedevskoye (Karelian Isthmus, Russia). Dokl. Earth Sci. 457:819–823.

Andronikov, A. V.; van Hoesel, A.; Andronikova, I. E.; and Hoek, W. Z. 2016*b*. Trace element distribution and implications in sediments across the Allerød–Younger Dryas boundary in the Netherlands and Belgium. Geogr. Ann. Ser. A Phys. Geogr. 98:325–345. doi:10.1111/geoa.12140.

Asher, D. J., and Clube, S. V. M. 1993. An extraterrestrial influence during the current glacial-interglacial. Q. J. R. Astron. Soc. 34:481–511.

Bard, E.; Hamelin, B.; and Delanghe-Sabatier, D. 2010. Deglacial meltwater pulse 1B and Younger Dryas sea levels revisited with boreholes at Tahiti. Science 327 (5970):1235–1237.

Belcher, C. M.; Collinson, M. E.; Sweet, A. R.; Hildebrand, A. R.; and Scott, A. C. 2003. Fireball passes and nothing burns—the role of thermal radiation in the Cretaceous-Tertiary event: evidence from the charcoal record of North America. Geology 31:1061–1064.

Bland, P. A., and Artemieva, N. A. 2006. The rate of small impacts on Earth. Meteorit. Planet. Sci. 41:607–631.

Boehnhardt, H. 2004. Split comets. *In* Festou, M. C.; Keller, H. U.; and Weaver, H. A., eds. Comets II. Tucson, University of Arizona Press, p. 301–316.

Bond, G. C., and Lotti, R. 1995. Iceberg discharges into the North Atlantic on millennial time scales during the last glaciation. Science 267(5200):1005–1010. doi:10.1126/science.267.5200.1005.

Boslough, M.; Harris, A. W.; Chapman, C.; and Morrison, D. 2013. Younger Dryas impact model confuses comet facts, defies airburst physics. Proc. Natl. Acad. Sci. USA 110(45):E4170. doi:10.1073/pnas.1313495110.

Broecker, W. S. 1997. Thermohaline circulation, the Achilles heel of our climate system: will man-made CO_2 upset the current balance? Science 278(5343):1582–1588.

Brook, E. J.; Bauska, T.; and Mix, A. 2015. Isotopic constraints on greenhouse gas variability during the last deglaciation from blue ice archives. *In* Sarnthein, M., and Haug, G. H., eds. Deglacial changes in ocean dynamics and atmospheric CO_2. Nova Acta Leopold. 121 (408):39–42.

Bunch, T. E.; Hermes, R. E.; Moore, A. M. T.; Kennett, D. J.; Weaver, J. C.; Wittke, J. H.; DeCarli, P. S.; et al. 2012. Very high-temperature impact melt products as evidence for cosmic airbursts and impacts 12,900 years ago [author summary]. Proc. Natl. Acad. Sci. USA 109:11,066–11,067.

Carlisle, D. B., and Braman, D. R. 1991. Nanometre-size diamonds in the Cretaceous/Tertiary boundary clay of Alberta. Nature 352:708–709.

Carlson, A. E. 2013. The Younger Dryas climate event. *In* Elias, S. A., ed. The encyclopedia of Quaternary science, vol. 3. Amsterdam, Elsevier, p. 126–134.

Clube, S. V. M., and Napier, W. M. 1984. The microstructure of terrestrial catastrophism. Mon. Notes R. Astron. Soc. 211:953–968.

Cooke, R. 1998. Human settlement of Central America and northernmost South America (14,000–8000 BP). Quat. Int. 49–50:177–190.

Crutzen, P.; Galbally, I. E.; and Brühl, C. 1984. Atmospheric effects from post-nuclear fires. Clim. Change 6:323–364.

de Angelis, M.; Steffensen, J. P.; Legrand, M.; Clausen, H.; and Hammer, C. 1997. Primary aerosol (sea salt and soil dust) deposited in Greenland ice during the last climatic cycle: comparison with east Antarctic records. J. Geophys. Res. Oceans 102(C12):26,681–26,698.

di Sisto, R. P.; Fernández, J. A.; and Brunini, A. 2009. On the population, physical decay and orbital distribution of Jupiter family comets: numerical simulations. Icarus 203:140–154.

Dubietis, A., and Arlt, R. 2007. Taurid resonant-swarm encounters from two decades of visual observations. Mon. Notes R. Astron. Soc. 376(2):890–894.

Eichler, A.; Tinner, T.; Brütsch, S.; Olivier, S.; Papina, T.; and Schwikowski, M. 2011. An ice-core based history of Siberian forest fires since AD 1250. Quat. Sci. Rev. 30:1027–1034.

Firestone, R. B.; West, A.; Kennett, J. P.; Becker, L.; Bunch, T. E.; Revay, Z. S.; Schultz, P. H.; et al. 2007. Evidence for an extraterrestrial impact 12,900 years ago that contributed to the megafaunal extinctions and the Younger Dryas cooling. Proc. Natl. Acad. Sci. USA 104:16,016–16,021.

Fischer, H.; Schüpbach, S.; Gfeller, G.; Bigler, M.; Röthlisberger, R.; Erhardt, T.; Stocker, T. F.; Mulvaney, R.;

and Wolff, E. W. 2015. Millennial changes in North American wildfire and soil activity over the last glacial cycle. Nat. Geosci. 8:723–727.

Florenskiy, K. P. 1965. Preliminary results from the 1961 combined Tunguska Meteorite Expedition. Spectrum Translation and Research, transl. http://abob.libs.uga.edu/bobk/tungmet.html. Originally published in Russian in 1963. Meteoritika 23:3–27.

Flynn, G. J.; Bleuet, P.; Borg, J.; Bradley, J. P.; Brenker, F. E.; Brennan, S.; Bridges, J.; et al. 2006. Elemental compositions of comet 81P/Wild 2 samples collected by Stardust. Science 314:1731–1735.

Fuhrer, K., and Legrand, M. 1997. Continental biogenic species in the Greenland Ice Core Project ice core: tracing back the biomass history of the North American continent. J. Geophys. Res. Oceans 102(C12): 26,735–26,745.

Gabrielli, P.; Barbante, C.; Plane, J. M. C.; Boutron, C. F.; Jaffrezo, J. L.; Mather, T. A.; Stenni, B.; et al. 2008. Siderophile metal fallout to Greenland from the 1991 winter eruption of Hekla (Iceland) and during the global atmospheric perturbation of Pinatubo. Chem. Geol. 255:78–86.

GERM (Geochemical Earth Reference Model) Reservoir Database. 2016. Data for Pt. https://earthref.org/GERMRD/.

Hahn, G., and Bailey, M. E. 1990. Rapid dynamical evolution of giant comet Chiron. Nature 348:132–136. doi:10.1038/348132a0.

Hasegawa, I. 1992. Historical variation in the meteor flux as found in Chinese and Japanese chronicles. Celest. Mech. Dyn. Astron. 54:129–142.

Hill, J. E. 1961. Problems of fire in nuclear warfare. Document P-2414. Santa Monica, CA, Rand, 32 p.

Hoyle, F. 1981. Ice. London, Hutchinson.

Hoyle, F., and Wickramasinghe, C. 1978. Comets, ice ages, and ecological catastrophes. Astrophys. Space Sci. 53: 523–526.

Jenniskens, P.; Nénon, Q.; Gural, P. S.; Albers, J.; Haberman, B.; Johnson, B.; Morales, R.; Grigsby, B. J.; Samuels, D.; and Johannink, C. 2016. CAMS newly detected meteor showers and the sporadic background. Icarus 266:384–409.

Kaiho, K.; Oshima, N.; Adachi, K.; Adachi, Y.; Mizukami, T.; Fujibayashi, M.; and Saito, R. 2016. Global climate change driven by soot at the K-Pg boundary as the cause of the mass extinction. Sci. Rep. 6:28427. doi: 10.1038/srep28427.

Kehrwald, N.; Zangrando, R.; Gabrielli, P.; Jaffrezo, J.-L.; Boutron, C.; Barbante, C.; and Gambaro, A. 2012. Levoglucosan as a specific marker of fire events in Greenland snow. Tellus B 64(1):18196. doi:10.3402/tellusb.v64i0.18196.

Kennett, J. P.; Kennett, D. J.; Culleton, B. J.; Aura Tortosa, J. E.; Bischoff, J. L.; Bunch, T. E.; Daniel, I. R., Jr.; et al. 2015. Bayesian chronological analyses consistent with synchronous age of 12,835–12,735 cal BP for Younger Dryas boundary on four continents. Proc. Natl. Acad. Sci. USA 112(32):E4344–4353.

Kennett, J. P.; Kennett, D. J.; LeCompte, M. A.; and West, A. 2018. Potential consequences of the YDB cosmic impact at 12.8 ka. *In* Goodyear, A. C., and Moore, C. R., eds. Early human life on the southeastern coastal plain. Gainesville, University Press of Florida, forthcoming.

Kinzie, C. R.; Que Hee, S. S.; Stich, A.; Tague, K. A.; Mercer, C.; Razink, J. J.; Kennett, D. J.; et al. 2014. Nanodiamond-rich layer across three continents consistent with major cosmic impact at 12,800 cal BP. J. Geol. 122(5):475–506.

Kirova, O. A., and Zaslavskaya, N. I. 1966. Data characterizing the dispersed matter as recovered from the area of fall of the Tunguska meteorite. Meteoritika 27:119–127 (in Russian).

Klekociuk, A. R.; Brown, P. G.; Pack, D. W.; ReVelle, D. O.; Edwards, W. N.; Spalding, R. E.; Tagliaferri, E.; Yoo, B. B.; and Zagari, J. 2005. Meteoritic dust from the atmospheric disintegration of a large meteoroid. Nature 436:1132–1135.

Kurbatov, A. V.; Mayewski, P. A.; Steffensen, J. P.; West, A.; Kennett, D. J.; Kennett J. P.; Bunch, T. E.; et. al. 2010. Discovery of a nanodiamond-rich layer in the Greenland ice sheet. J. Glaciol. 56:747–757.

Legrand, M. R.; de Angelis, M.; Staffelbach, T.; Neftel, A.; and Stauffer, B. 1992. Large perturbations of ammonium and organic acids content in the Summit-Greenland ice core. Fingerprint from forest fires? Geophys. Res. Lett. 19:473–475.

Legrand, M.; McConnell, J.; Fischer, H., Wolff, E. W.; Preunkert, S.; Arienzo, M.; Chellman, N.; et al. 2016. Boreal fire records in Northern Hemisphere ice cores: a review. Clim. Past 12:2033–2059.

Manchester, C. W., and Patterson, W. P. 2008. Climate change during the Late Glacial and early Holocene from Lough Monreagh, western Ireland: evidence from carbon and oxygen isotope values of lacustrine marl. EOS: Trans. Am. Geophys. Union 89(53), Fall Meeting suppl., abstract PP13C-1457.

Mayewski, P. A.; Meeker, L. D.; Twickler, M. S.; Whitlow, S.; Yang, Q.; Lyons, W. B.; and Prentice, M. 1997. Major features and forcing of high-latitude Northern Hemisphere atmospheric circulation using a 110,000-year-long glaciochemical series. J. Geophys. Res. Oceans 102(C12):26,345–26,366.

Mayewski, P. A.; Meeker, L. D.; Whitlow, S.; Twickler, M. S.; Morrison, M. C.; Alley, R. B.; Bloomfield, P.; and Taylor, K. 1993. The atmosphere during the Younger Dryas. Science 261(5118):195–197.

Mayewski, P. A.; Twickler, M. S.; Whitlow, S. I.; Meeker, L. D.; Yang, Q.; Thomas, J.; Kreutz, K.; et al. 1996. Climate change during the last deglaciation in Antarctica. Science 272:1636–1638.

Meese, D. A.; Gow, A. J.; Alley, R. B.; Zielinski, G. A.; Grootes, P. M.; Ram, M.; Taylor, K. C.; Mayewski, P. A.; and Bolzan, J. F. 1997. The Greenland Ice Sheet Project 2 depth-age scale: methods and results. J. Geophys. Res. Oceans 102(C12):26411–26423.

Melott, A.; Thomas, B. C.; Dreschhoff, G.; and Johnson, C. K. 2010. Cometary airbursts and atmospheric

chemistry: Tunguska and a candidate Younger Dryas event. Geology 38:355–358. doi:10.1130/G30508.1.
Melott, A. L.; Thomas, B. C.; Laird, C. M.; Neuenswander, B.; and Atri, D. 2016. Atmospheric ionization by high-fluence, hard-spectrum solar proton events and their probable appearance in the ice core archive. J. Geophys. Res. Atmos. 121(6):3017–3033. doi:10.1002/2015JD024064.
Menviel, L.; Mouchet, A.; Meissner, J. K.; Joos, F.; and England, M. H. 2015. Impact of oceanic circulation changes on atmospheric $\delta^{13}CO_2$. Glob. Biogeochem. Cycles 29:1944–1961.
Mills, M. J.; Toon, O. B.; Lee-Taylor, J.; and Robock, A. 2014. Multidecadal global cooling and unprecedented ozone loss following a regional nuclear conflict. Earth's Future 2:161–176.
Moore, C. R.; West, A.; LeCompte, M. A.; Brooks, M. J.; Daniel, I. R., Jr.; Goodyear, A. C.; Ferguson, T. A.; et al. 2017. Widespread platinum anomaly documented at the Younger Dryas onset in North American sedimentary sequences. Sci. Rep. 7:44031. doi:10.1038/srep44031.
Napier, W. M. 2010. Palaeolithic extinctions and the Taurid Complex. Mon. Notes R. Astron. Soc. 405: 1901–1906.
———. 2015. Giant comets and mass extinctions of life. Mon. Notes R. Astron. Soc. 448:27–36.
Napier, W. M.; Asher, D. J.; Bailey, M. E.; and Steel, D. I. 2015. Centaurs as a hazard to civilization. Astron. Geophys. 56:6.24–6.30. doi:10.1093/astrogeo/atv198.
Napier, W. M.; Bunch, T. E.; Kennett, J. P.; Wittke, J. H.; Tankersley, K. B.; Kletetschka, G.; Howard, G. A.; and West, A. 2013. Reply to Boslough et al.: decades of comet research counter their claims. Proc. Natl. Acad. Sci. USA 110(45):E4171. doi:10.1073/pnas.1315467110.
National Research Council. 1985. The effects on the atmosphere of a major nuclear exchange. Washington, DC, National Academy Press, 93 p.
Neale, P. J., and Thomas, B. C. 2016. Solar irradiance changes and phytoplankton productivity in Earth's ocean following astrophysical ionizing radiation events. Astrobiology 16(4):245–258. doi:10.1089/ast.2015.1360.
O'Hara, Fred, Jr., ed. 1990. Glossary: carbon dioxide and climate. ORNL/CDIAC-39 (3rd ed.). Oak Ridge, TN, Carbon Dioxide Information Analysis Center, Oak Ridge National Laboratory.
Parkos, D.; Alexeenko, A.; Kulakhmetov, M.; Johnson, B. C.; and Melosh, H. J. 2015. NO_x production and rainout from Chicxulub impact ejecta reentry. J. Geophys. Res. Planets 120(12):2152–2168.
Petaev, M. I.; Huang, S.; Jacobsen, S. B.; and Zindler, A. 2013. Large Pt anomaly in the Greenland ice core points to a cataclysm at the onset of Younger Dryas. Proc. Natl. Acad. Sci. USA 110(32):12,917–12,920.
Pierazzo, E.; Garcia, R. R.; Kinnison, D. E.; Marsh, D. R.; Lee-Taylor, J.; and Crutzen, P. J. 2010. Ozone perturbation from medium-size asteroid impacts in the ocean. Earth Planet. Sci. Lett. 299(3–4):263–272.
Power, M. J.; Marlon, J.; Ortiz, N.; Bartlein, P. J.; Harrison, S. P.; Mayle, F. E.; Ballouche, A.; et. al. 2008. Changes in fire regimes since the Last Glacial Maximum: an assessment based on a global synthesis and analysis of charcoal data. Clim. Dyn. 30(7–8):887–907.
Ram, M., and Koenig, G. 1997. Continuous dust concentration profile of pre-Holocene ice from the Greenland Ice Sheet Project 2 ice core: dust stadials, interstadials, and the Eemian. J. Geophys. Res. Oceans 102(C12):26,641–26,648.
Rasmussen, S. O.; Seierstad, I. K.; Andersen, K. K.; Bigler, M.; Dahl-Jensen, D.; and Johnsen, S. J. 2008. Synchronization of the NGRIP, GRIP, and GISP2 ice cores across MIS 2 and palaeoclimatic implications. Quat. Sci. Rev. 27:18–28.
Reach, W. T.; Kelley, M. S.; and Sykes, M. V. 2007. A survey of debris trails from short-period comets. Icarus 191:298–322.
Renssen, H.; Mairesse, A.; Goosse, H.; Mathiot, P.; Heiri, O.; Roche, D. M.; Nisancioglu, K. H.; and Valdes, P. J. 2015. Multiple causes of the Younger Dryas cold period. Nat. Geosci. 8(12):946–949.
Robertson, D. S.; McKenna, M. C.; Toon, O. B.; Hope, S.; and Lillegraven, J. A. 2004. Fireball passes and nothing burns—the role of thermal radiation in the Cretaceous-Tertiary event: evidence from the charcoal record of North America: comment and reply. Geology 32(1):e50.
Rudnick, R. L., and Gao, S. 2003. Composition of the continental crust. *In* Rudnick, R. L., ed. The crust. Vol. 3 of Holland, H. H., and Turekian, K. K., eds. Treatise on geochemistry. Oxford, Pergamon, p. 1–64.
Santín, C.; Doerr, S. H.; Kane, E. S.; Masiello, C. A.; Ohlson, M.; de la Rosa, J. M.; Preston, C. M.; and Dittmar, T. 2016. Towards a global assessment of pyrogenic carbon from vegetation fires. Glob. Change Biol. 22:76–91. doi:10.1111/gcb.12985.
Seierstad, I. K.; Abbott, P. M.; Bigler, M.; Blunier, T.; Bourne, A. J.; Brook, E.; Buchardt, S. L.; et al. 2014. Consistently dated records from the Greenland GRIP, GISP2 and NGRIP ice cores for the past 104 ka reveal regional millennial-scale $\delta^{18}O$ gradients with possible Heinrich event imprint. Quat. Sci. Rev. 106:29–46.
Shaw, J. 2002. The meltwater hypothesis for subglacial bedforms. Quat. Int. 90:5–22.
Steel, D. I., and Asher, D. J. 1996. The orbital dispersion of the macroscopic Taurid objects. Mon. Notes R. Astron. Soc. 280:806–822.
Steffensen, J. P.; Andersen, K. K.; Bigler, M.; Clausen, H. B.; Dahl-Jensen, D.; Fischer, H.; Goto-Azuma, K.; et. al. 2008. High-resolution Greenland ice core data show abrupt climate change happens in few years. Science 321:680–684.
Still, C. J.; Berry, J. A.; Collatz, G. J.; and Defries, R. S. 2003. Global distribution of C_3 and C_4 vegetation: carbon cycle implications. Glob. Biogeochem. Cycles 17(1):1006. doi:10.1029/2001GB001807.
Stuiver, M.; Grootes, P. M.; and Braziunas, T. F. 1995. The GISP2 $\delta^{18}O$ climate record of the past 16,500 years and the role of the sun, ocean, and volcanoes. Quat. Res. 44:341–354.

Taylor, K. C.; Mayewski, P. A.; Twickler, M. S.; and Whitlow, S. I. 1996. Biomass burning recorded in the GISP2 ice core: a record from eastern Canada? Holocene 6(1):1–6.

Teller, J. T. 2013. Lake Agassiz during the Younger Dryas. Quat. Res. 80(3):361–369.

Thomas, B. C.; Goracke, B. D.; and Dalton, S. M. 2016. Atmospheric constituents and surface-level UVB: implications for a paleoaltimetry proxy and attempts to reconstruct UV exposure during volcanic episodes. Earth Planet. Sci. Lett. 453(1):141–151. doi:10.1016/j.epsl.2016.08.014.

Thomas, B. C.; Neale, P. J.; and Snyder, B. R., II. 2015. Solar irradiance changes and photobiological effects at Earth's surface following astrophysical ionizing radiation events. Astrobiology 15(3):207–220. doi:10.1089/ast.2014.1224.

Whitlow, S. I.; Mayewski, P. A.; Dibb, J.; Holdsworth, G.; and Twickler, M. S. 1994. An ice-core-based record of biomass burning in North America. Tellus B 46:234–242.

Wiegert, P.; Vaubaillon, J.; and Campbell-Brown, M. 2009. A dynamical model of the sporadic meteoroid complex. Icarus 201:295–310.

Wolbach, W. S., and Anders, E. 1989. Elemental carbon in sediments: determination and isotopic analysis in the presence of kerogen. Geochim. Cosmochim. Acta 53:1637–1647.

Wolbach, W. S.; Ballard, J. P.; Mayewski, P. A.; Parnell, A. C.; Cahill, N.; Adedeji, V.; Bunch, T. E.; et al. 2018. Extraordinary biomass-burning episode and impact winter triggered by the Younger Dryas cosmic impact ~12,800 years ago. 2. Lake, marine, and terrestrial sediments. J. Geol. 126:XXX–XXX.

Wu, Y.; Sharma, M.; LeCompte, M. A.; Demitroff, M.; and Landis, J. 2013. Origin and provenance of spherules and magnetic grains at the Younger Dryas boundary. Proc. Natl. Acad. Sci. USA 110(38):E3557–E3566.